
# CLEEN Phase III Sustainable Aviation Fuels Project: UDRI Phase 2 Test Report

FAA/Boeing Continuous Lower Energy, Emissions, and Noise (CLEEN)
Phase III Technology Demonstration Program

Cooperative Agreement # 693KA9 – 21 – T – 00001
September 30, 2024

Prepared for:

Arthur Orton
CLEEN Phase III Program Manager
Federal Aviation Administration
800 Independence Ave, S.W.
Washington, DC 20591

Presented by:
Ilya Kosilkin (PI) Phone Number: (425) 239-9481 Email: ilya.v.kosilkin@boeing.com

Contracts Administrator: Lindsay Von Hatten
Phone Number: (314) 563-7434
Email: lindsay.e.vonhatten@boeing.com



*The Boeing Company*
PO Box 516, M/C S102-2067, Saint Louis, MO 63166

# Introduction

This report was prepared under Federal Aviation Administration (FAA) Other Transaction Agreement (OTA) 693KA9 – 21 – T – 00001, Continuous Lower Energy, Emissions and Noise Technologies Program - Phase III (CLEEN III) as part of the CLEEN III Sustainable Aviation Fuels (SAF) project. It reflects the efforts performed under contract to Boeing by the University of Dayton Research Institute (UDRI), with the primary objective being the generation of appropriate data for understanding variability of properties of nitrile rubber with fuels containing various aromatic and cycloparaffinic content.

To accomplish the goals of this project, the CLEEN III SAF project comprises two phases of laboratory testing conducted by UDRI. The report herein covers the second and final phase of the effort. Results of the first phase of the project have been previously posted to the FAA CLEEN program website and can be found at https://www.faa.gov/media/78041

The objectives of the Phase 2 effort were to investigate the compatibility of nitrile butadiene rubber O-rings with cycloparaffinic test fluids, examine leak characteristics of O-rings that were previously aged during Phase 1 of the project and to study O-ring compressive stress relaxation. The Phase 1 report provides detailed information on the O-rings used throughout this CLEEN III SAF project, their initial performance, aging conditions, test fluid selection (including composition), test parameters, and method descriptions.

Note that the work presented in both reports completes the UDRI efforts performed under the CLEEN III SAF project and is provided to expand on our collective understanding of how sustainable aviation fuels without aromatics effect the nitrile rubber O-rings pervasive in current and legacy aircraft. The Boeing CLEEN III team thanks the UDRI project team for their participation in the SAF project and for expanding this understanding, building on work they have pursued over many years.

At the completion of the Boeing CLEEN phase III program, a final report will be published that summarizes all efforts conducted under the CLEEN III SAF project.

As a further note, both the UDRI Phase 1 and Phase 2 reports reference “compression %” and “compression set %” as primary parameters of interest during laboratory testing. These parameters are determined in accordance with ASTM D395, with the only variance being the use of UDRI test fixtures.

University of Dayton Research Institute

September 5, 2024

# Final Report

# Material Compatibility Testing for CLEEN III Phase 2 Summary Report

## Report Number: UDR-TR-2024-90
## Proposal No. R-25894
## PO No. 2145658

**Prepared for:**

The Boeing Company

Ilya Kosilkin
ilya.v.kosilkin@boeing.com

**Prepared by:**

University of Dayton Research Institute
300 College Park
Dayton, OH 45469

John L. Graham, Ph.D.
Distinguished Research Engineer
John.Graham@udri.udayton.edu

Gina C. Roesch, Ph.D.
Associate Research Chemist
Gina.Roesch@udri.udayton.edu

**BACKGROUND**

In 2003 the University of Dayton Research Institute (UDRI) began a program with the Air Force Research Laboratory (AFRL) in support of the United States Department of Defense (DOD) Flexible JP-8 Program. This program was designed to investigate the development and fielding of jet turbine fuels derived from non-petroleum sources such as coal and biomass. A major concern with these fuels was that they were often compositionally different than conventional fuels and that they may not be compatible with all of the materials in a modern fuel system that have evolved to accommodate petroleum distillate fuels. Of primary concern was the role of aromatic components which were known to interact with fuel system elastomers and these components were often absent from the alternative jet turbine fuel being developed. While there was considerable evidence that the levels of aromatics in jet turbine fuel could have a significant impact on material compatibility as well as fuel performance, there was little detailed information on the specific role of aromatics in material compatibility in general and its impact on the performance of O-ring seals in particular.

The initial effort executed by UDRI in support of AFRL was to develop a fundamental understanding of exactly how jet turbine fuels in general, and the aromatics in particular, interact with polymeric fuel system materials. This work was successful and a detailed understanding of how all of the major fuel components interact with fuel system polymers was obtained. Furthermore, a unique set of laboratory, data analysis, and computational tools were developed to support this research. In 2006 these research tools were employed as testing tools to support the first flight tests of 50% alternative fuel blends and later were used as screening tools as part of the Tier 2 and Tier 3 material compatibility testing protocol developed in support of ASTM D4054.

In 2009 UDRI began an effort in support of The Boeing Company's participation in the FAA's CLEEN program. This effort examined the fluid compatibility of synthetic paraffinic kerosene (SPK) fuels and SPK/Jet A fuel blends with selected polymeric materials found in commercial aircraft. This effort also expanded earlier work which suggested that SPK fuels that were high in cycloparaffins could offer enhanced material compatibility and reduced reliance on aromatic components. (See J. Graham, T. Rahmes, M. Kay, J. Belières, J. Kinder, S. Millett, J. Ray, W. Vannice, J. Trela, "Evaluating the Impact of SPK Fuels and Fuel Blends on Non-metallic Materials used in Commercial Aircraft Fuel Systems," DTFA WA-10-C-0030, Final Report, The Boeing Company, Seattle, WA, December 2013.)

In 2013 UDRI began a series of programs for the Defense Logistics Agency (DLA) to examine the impact of the intermittent use of SPK/JP-8 fuel blends on the performance of O-ring seals. This work expanded the testing and evaluation capabilities to include component-level work under representative service conditions and resulted in the development of new test methods to evaluate the effects of alterative jet turbine fuels on the short-term behavior of O-rings seals; principally the changes that occur within the first 7 days following the switching between a conventional jet turbine fuel and a low-aromatic SPK/JP-8 fuel blend (fuel switch-loading). These results showed that O-ring seals were very robust and should tolerate a low-aromatic SPK/JP-8 fuel blends until the seals are near the end of their service life.
The body of previous work indicated that nitrile rubber O-ring seals will likely present the

greatest challenge to the implementation of a low-aromatic SPK/JP-8 fuel blends as this material shows the greatest response to changes in fuel composition.

Launched in 2021 as part of the Boeing CLEEN phase III program, the primary objective of the proposed work was to generate appropriate data for understanding variability of properties of nitrile rubber with fuels containing various aromatic and cycloparaffinic content. This evaluation included an assessment of the fluid compatibility in a manner described in previous work, as well as chronic effects on function critical physical properties, most notably compression set and compressive stress relaxation and its influence on sealing performance. The collected data will be used to help establish a base line for material properties and to more precisely define conditions for testing with synthetic aviation fuels with high cycloparaffin content. Therefore, an additional objective of the project is to predict compatibility of zero aromatic, high cycloparaffin content synthetic fuels with new and aged aircraft fuel systems.

To accomplish the goals of this project a program consisting of 6 technical tasks as listed in Table 1 was proposed. As shown, these tasks are grouped as Tasks 1-3 in Phase 1 and 4-6 in Phase 2. The pages that follow summarize the results from Phase 2.

**Table 1 – Technical Tasks**

| Phase | Task | Description |
|---|---|---|
| 1 | 1 | Material Acquisition and Baseline Testing |
| | 2 | Compression, Compression Set, and Volume Swell |
| | 3 | Compression and Compression Set with fuel Switch-loading |
| 2 | 4 | Compression and Compression Set with Cycloparaffinic Fuels |
| | 5 | Optical Cell Leak Testing |
| | 6 | Compressive Stress Relaxation with Thermal Cycling |

## RESULTS AND DISCUSSION

### Task 4 - Compression and Compression Set with Cycloparaffinic Fuels

In this task the compression and compression set were measured for selected test materials while being compressed 25% (nominal) in the UDRI compression fixtures (see Figure 1) at 160˚F. The test fluids included SPK/CPK-0 fuel blends with 20%, 50%, 80%, and 100% CPK-0. These tests also included a set of samples in which the fuel was periodically switched between a mid-range Jet A with 16.2% aromatics (Jet A_16) and the CPK-0 fuel. The O-rings used for this task included N0602, N400, and 4475, all qualified to AMS-P-5315. During this task the compression and compression set was measured every 2 weeks over a period of 26 weeks in accordance with ASTM D395 with the variance that the UDRI fixtures were used. For the O-rings in which the fuel was periodically switched between the Jet A_16 and the CPK-0, this switch occurred every 2 weeks as the testing was paused so that the compression and compression set of the O-rings could be measured. At the conclusion of the aging period the tests listed in Table 2 were performed.

**Table 2 – Task 4 Post-run Tests**

| Property | Method | Notes |
|---|---|---|
| Hardness, Type M | ASTM D2240 | Shore M |
| Tensile | ASTM D1414 | Tensile Strength |
| Elongation | ASTM D1414 | Ultimate Elongation |
| Modulus | ASTM D1414 | Concurrent with ASTM D1414 |
| IR Spectrum | ATR | Attenuated Total Reflectance |
| Glass Transition | ASTM E1545 | Thermomechanical Analysis |

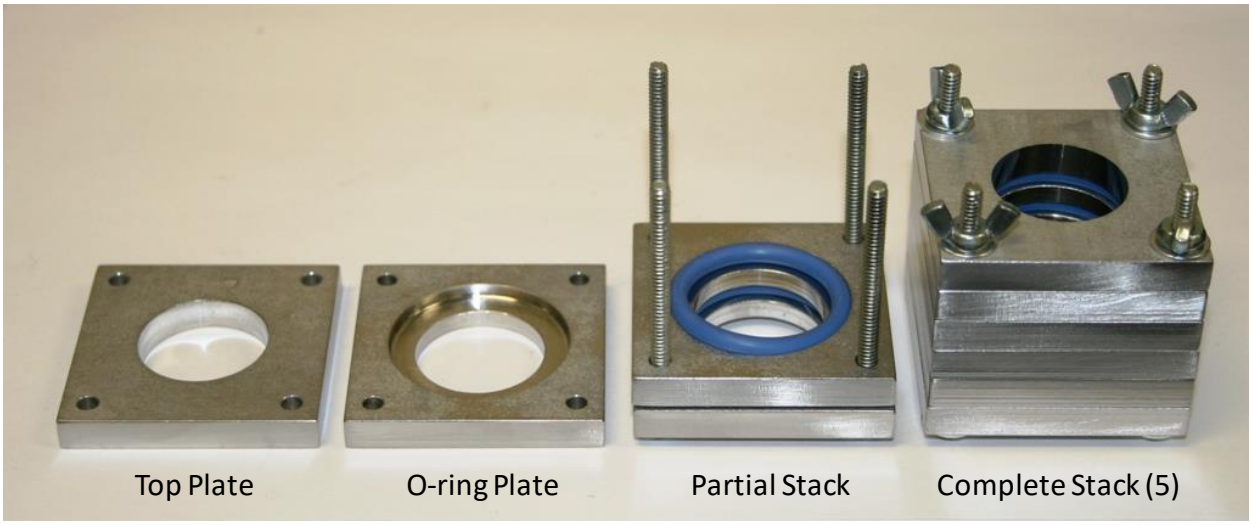


**Figure 1. The UDRI compression set fixtures designed to constrain O-rings in a model gland to mimic the conditions of an internally pressurized seal and produce aged samples that will fit in the UDRI O-ring flow and optical cells.**

The test results expressed in terms of compression are summarized in Tables 3-5. The compression test results for the exposures to a single fuel are summarized in Figures 2-4 and the results from the switch-loading are summarized in Figures 5-7. Similarly, the test results in terms of compression set are summarized in Tables 6-8 and the compression set results for the exposures to a single fuel are summarized in Figures 8-10 and for the switch-loading in Figures 11-13. Note that the compression results for Jet A_16 from Task 2 are included in the tables for comparison. Overall, these results show that the behavior tracks the volume swell in that as the level of CPK-0 in SPK increases the volume swell increases, the measured compression increases, and the measured compression set decreases. Furthermore, the overall temporal behavior for each fuel is similar as illustrated by the curves essentially being parallel to each other. That is, the rate of change in the compression and compression set is not influenced by the CPK-0 content. Similarly, given that the volume swell of the CPK-0 compares well with the Jet A_16 switch-loading between these two fuels had little effect on the compression and compression set.

**Table 3 – N0602 Measured Compression, %**

| Weeks | 20% CPK-0 | 50% CPK-0 | 80% CPK-0 | CPK-0 | Jet A_16* | Jet A_16 | CPK-0 |
|---|---|---|---|---|---|---|---|
| 0 | 23.9 | 23.7 | 23.8 | 23.7 | 26.1 | 23.6 | 23.6 |
| 2 | 18.5 | 19.4 | 20.4 | 21.3 | 21.1 | 21.1 | |
| 4 | 17.3 | 18.1 | 18.8 | 20.0 | 19.7 | | 19.5 |
| 6 | 15.7 | 17.0 | 17.9 | 18.8 | 18.5 | 18.6 | |
| 8 | 14.8 | 16.1 | 17.1 | 18.1 | 17.8 | | 17.5 |
| 10 | 13.9 | 15.2 | 16.7 | 17.5 | 17.3 | 17.3 | |
| 12 | 13.3 | 14.6 | 15.8 | 16.9 | 16.6 | | 16.4 |
| 14 | 12.7 | 13.9 | 15.1 | 16.3 | 15.7 | 16.0 | |
| 16 | 11.9 | 13.4 | 14.3 | 15.8 | 15.1 | | 14.9 |
| 18 | 11.4 | 12.6 | 13.6 | 15.1 | 14.5 | 14.7 | |
| 20 | 10.7 | 12.0 | 13.2 | 14.5 | 14.1 | | 13.7 |
| 22 | 10.5 | 11.5 | 12.8 | 13.7 | 13.3 | 13.3 | |
| 24 | 10.0 | 11.1 | 12.4 | 13.5 | 12.7 | | 12.5 |
| 26 | 9.4 | 10.6 | 11.9 | 13.1 | 12.2 | 12.3 | |

*From Task 2

**Table 4 – N400 Measured Compression, %**

| Weeks | 20% CPK-0 | 50% CPK-0 | 80% CPK-0 | CPK-0 | Jet A_16* | Jet A_16 | CPK-0 |
|---|---|---|---|---|---|---|---|
| 0 | 23.9 | 23.6 | 23.8 | 23.7 | 26.1 | 23.6 | 23.6 |
| 2 | 18.7 | 19.1 | 19.9 | 20.6 | 21.0 | 20.9 | |
| 4 | 17.5 | 17.9 | 18.3 | 19.3 | 19.6 | | 19.1 |
| 6 | 16.3 | 16.8 | 17.6 | 18.1 | 18.7 | 18.5 | |
| 8 | 15.5 | 16.0 | 16.8 | 17.5 | 18.0 | | 17.4 |
| 10 | 14.9 | 15.4 | 16.4 | 16.9 | 17.5 | 17.4 | |
| 12 | 14.4 | 14.6 | 15.6 | 16.2 | 17.0 | | 16.5 |
| 14 | 13.8 | 14.1 | 15.1 | 15.8 | 16.4 | 16.2 | |
| 16 | 13.0 | 13.6 | 14.3 | 15.2 | 15.5 | | 15.4 |
| 18 | 12.9 | 13.0 | 13.7 | 14.6 | 15.0 | 15.2 | |
| 20 | 12.2 | 12.5 | 13.4 | 14.2 | 14.6 | | 14.3 |
| 22 | 12.0 | 12.2 | 13.4 | 13.5 | 13.8 | 14.0 | |
| 24 | 11.7 | 11.9 | 12.9 | 13.3 | 13.4 | | 13.4 |
| 26 | 11.4 | 11.5 | 12.5 | 12.9 | 13.2 | 13.4 | |

*From Task 2

**Table 5 – 4457 Measured Compression, %**

| Weeks | 20% CPK-0 | 50% CPK-0 | 80% CPK-0 | CPK-0 | Jet A_16* | Jet A_16 | CPK-0 |
|---|---|---|---|---|---|---|---|
| 0 | 23.8 | 23.7 | 23.7 | 23.5 | 25.2 | 23.6 | 23.6 |
| 2 | 19.1 | 19.7 | 20.5 | 21.0 | 20.8 | 21.2 | |
| 4 | 18.1 | 18.7 | 19.6 | 20.0 | 19.9 | | 20.2 |
| 6 | 17.4 | 18.1 | 18.9 | 19.4 | 19.1 | 19.8 | |
| 8 | 16.8 | 17.6 | 18.4 | 18.7 | 18.7 | | 19.3 |
| 10 | 16.3 | 17.1 | 18.1 | 18.4 | 18.1 | 18.9 | |
| 12 | 15.9 | 16.5 | 17.6 | 17.9 | 17.7 | | 18.4 |
| 14 | 15.4 | 16.2 | 17.2 | 17.5 | 17.0 | 18.0 | |
| 16 | 14.8 | 15.7 | 16.7 | 17.1 | 16.3 | | 17.4 |
| 18 | 14.4 | 15.3 | 16.1 | 16.7 | 15.8 | 17.1 | |
| 20 | 13.8 | 14.9 | 15.8 | 16.1 | 15.5 | | 16.5 |
| 22 | 13.6 | 14.5 | 15.6 | 15.6 | 14.9 | 16.3 | |
| 24 | 13.4 | 14.2 | 15.3 | 15.3 | 14.4 | | 15.7 |
| 26 | 13.0 | 13.9 | 14.8 | 15.0 | 13.8 | 15.5 | |

*From Task 2

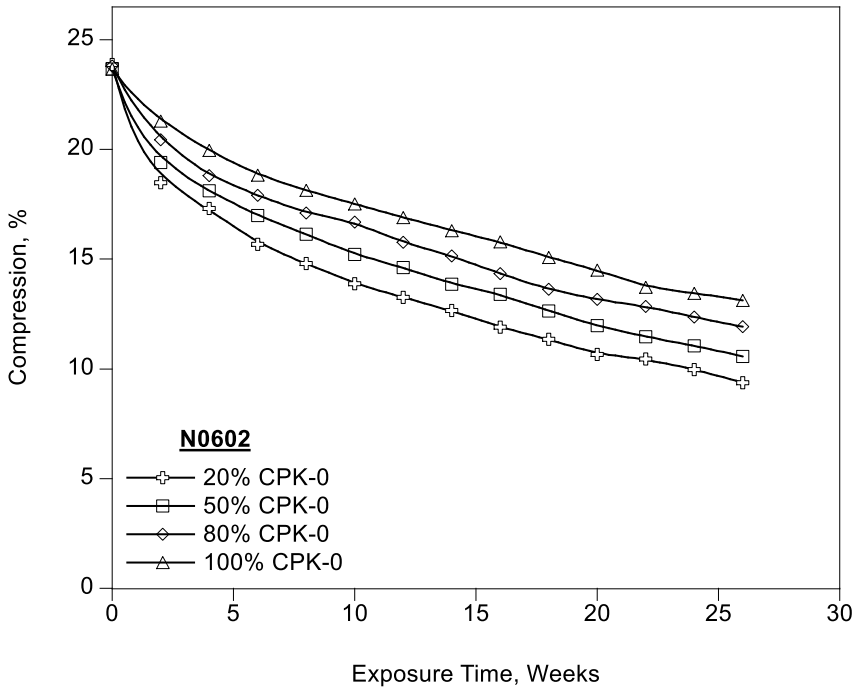


**Figure 2. The average compression of the N0602 O-rings in the test fuels.**

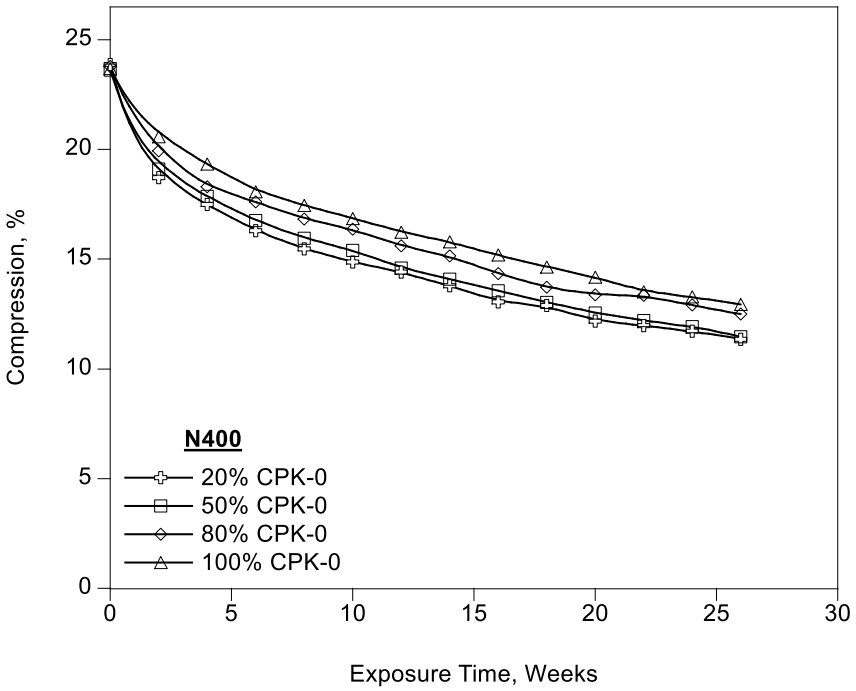


**Figure 3. The average compression of the N400 O-rings in the test fuels.**

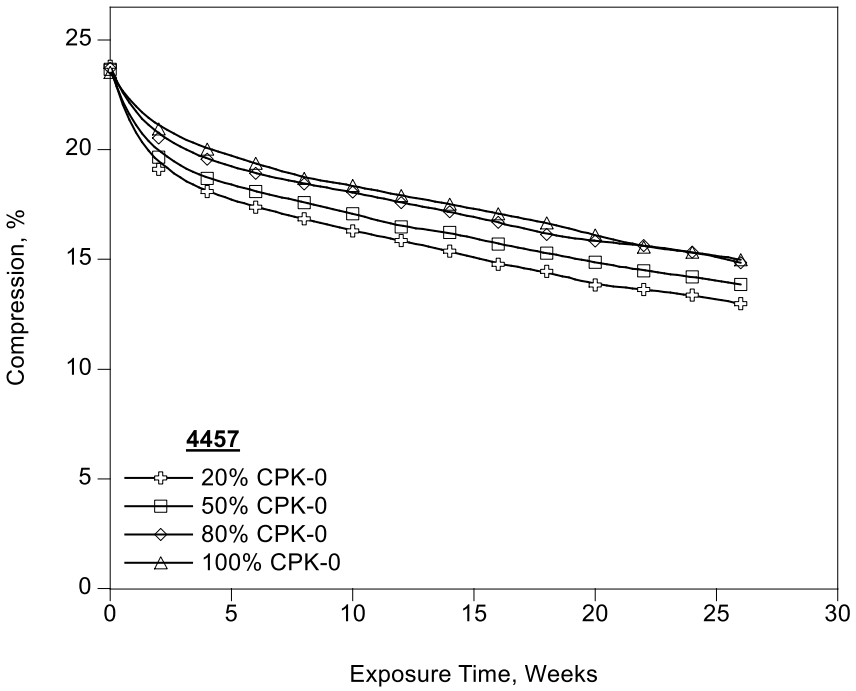


**Figure 4. The average compression of the 4457 O-rings in the test fuels.**

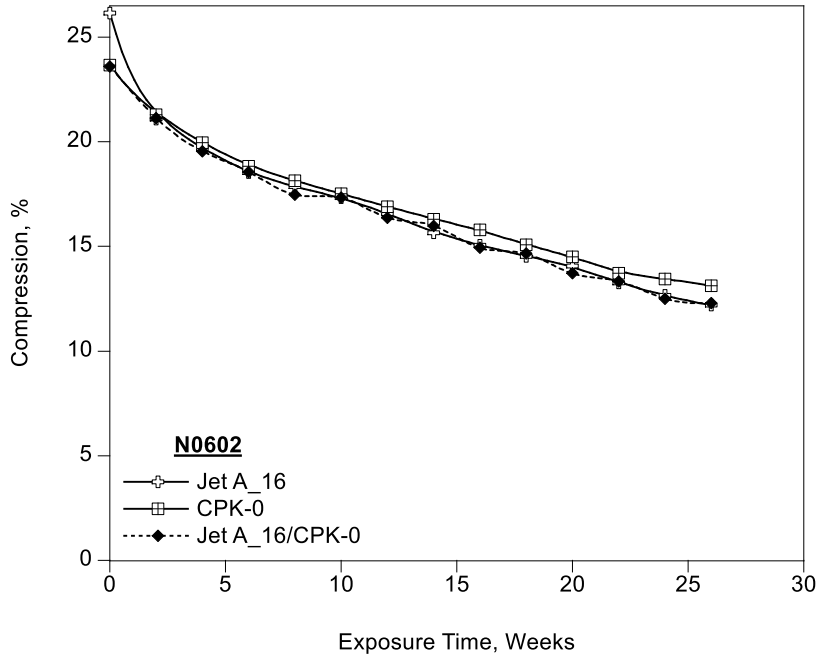


**Figure 5. Compression as a function of time for N0602 O-rings when exposed to a single fuel (Jet A_16 or CPK-0) and periodically switched between Jet A_16 and CPK-0. Note that the switch-load data points are joined using a cubic spline fit and this curve may not reflect the true temporal behavior.**

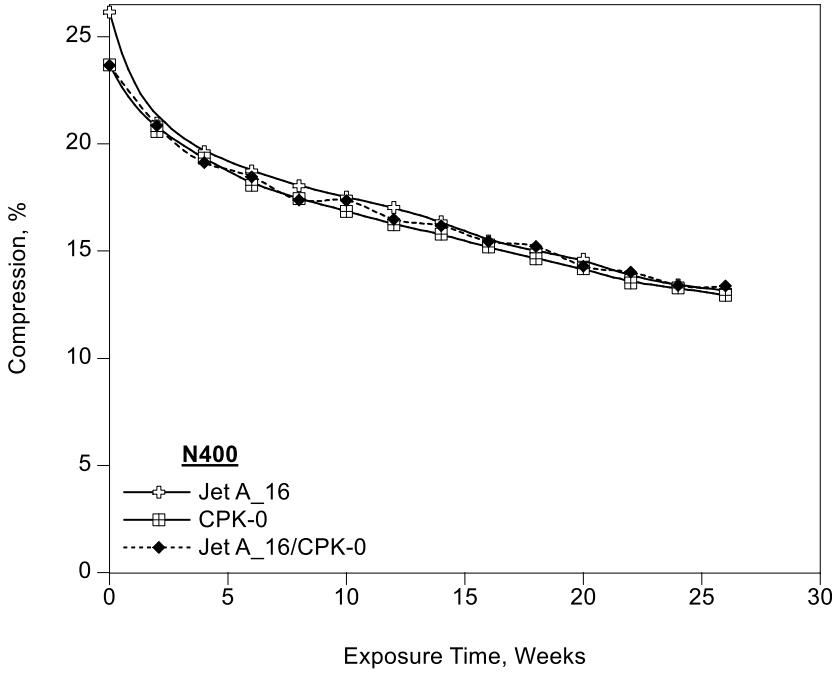


**Figure 6. Compression as a function of time for N400 O-rings when exposed to a single fuel (Jet A_16 or CPK-0) and periodically switched between Jet A_16 and CPK-0. Note that the switch-load data points are joined using a cubic spline fit and this curve may not reflect the true temporal behavior.**

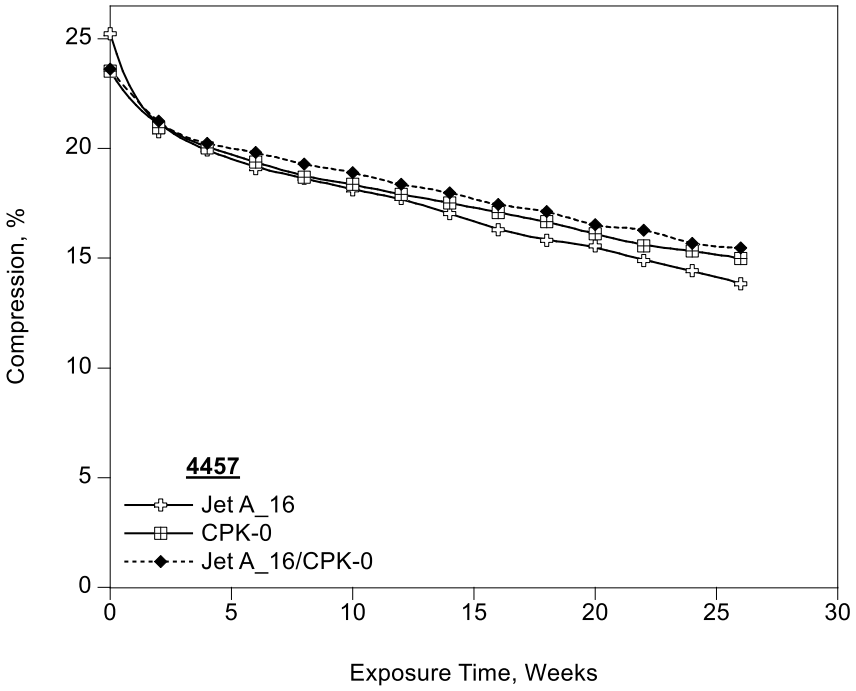


**Figure 7. Compression as a function of time for 4457 O-rings when exposed to a single fuel (Jet A_16 or CPK-0) and periodically switched between Jet A_16 and CPK-0. Note that the switch-load data points are joined using a cubic spline fit and this curve may not reflect the true temporal behavior.**

**Table 6 – N0602 Measured Compression Set, %**

| Weeks | 20% CPK-0 | 50% CPK-0 | 80% CPK-0 | 100% CPK-0 | Jet A_16 | Jet A_16 | CPK-0 |
|---|---|---|---|---|---|---|---|
| 0 | 0.0 | 0.0 | 0.0 | 0.0 | 0.0 | 0.0 | 0.0 |
| 2 | 27.7 | 22.3 | 17.8 | 12.6 | 14.0 | 13.2 | |
| 4 | 33.2 | 28.6 | 25.8 | 19.5 | 21.1 | | 21.3 |
| 6 | 40.6 | 33.9 | 30.2 | 25.1 | 26.8 | 26.2 | |
| 8 | 44.6 | 37.8 | 33.9 | 28.5 | 30.1 | | 31.5 |
| 10 | 48.6 | 42.1 | 35.9 | 31.5 | 32.5 | 32.1 | |
| 12 | 51.2 | 44.7 | 40.1 | 34.3 | 36.1 | | 36.6 |
| 14 | 53.7 | 47.9 | 42.8 | 37.1 | 40.2 | 38.4 | |
| 16 | 56.9 | 49.9 | 46.4 | 39.4 | 43.0 | | 43.1 |
| 18 | 59.1 | 53.3 | 49.5 | 42.7 | 45.3 | 44.4 | |
| 20 | 61.9 | 56.0 | 51.5 | 45.2 | 47.3 | | 48.5 |
| 22 | 62.7 | 58.1 | 52.8 | 48.6 | 50.8 | 50.1 | |
| 24 | 64.6 | 59.8 | 54.8 | 49.8 | 53.4 | | 53.7 |
| 26 | 67.0 | 61.8 | 56.7 | 51.2 | 55.3 | 54.6 | |

**Table 7 – N400 Measured Compression Set, %**

| Weeks | 20% CPK-0 | 50% CPK-0 | 80% CPK-0 | 100% CPK-0 | Jet A_16 | Jet A_16 | CPK-0 |
|---|---|---|---|---|---|---|---|
| 0 | 0.0 | 0.0 | 0.0 | 0.0 | 0.0 | 0.0 | 0.0 |
| 2 | 25.4 | 23.6 | 18.9 | 16.2 | 15.0 | 13.7 | |
| 4 | 31.3 | 29.6 | 27.0 | 22.5 | 21.7 | | 22.6 |
| 6 | 36.8 | 34.9 | 30.4 | 28.6 | 26.1 | 25.8 | |
| 8 | 40.6 | 38.6 | 34.1 | 31.6 | 29.5 | | 31.2 |
| 10 | 43.3 | 41.1 | 36.3 | 34.4 | 32.0 | 31.2 | |
| 12 | 45.4 | 44.7 | 39.8 | 37.3 | 34.2 | | 35.4 |
| 14 | 48.1 | 47.0 | 41.9 | 39.3 | 37.3 | 36.8 | |
| 16 | 51.3 | 49.2 | 45.4 | 42.1 | 41.3 | | 40.2 |
| 18 | 52.0 | 51.5 | 48.2 | 44.5 | 43.4 | 41.2 | |
| 20 | 55.0 | 53.6 | 49.6 | 46.5 | 45.1 | | 45.4 |
| 22 | 55.8 | 55.0 | 49.8 | 49.4 | 48.6 | 46.6 | |
| 24 | 57.0 | 56.2 | 51.7 | 50.5 | 50.3 | | 49.4 |
| 26 | 58.4 | 58.1 | 53.5 | 51.9 | 51.4 | 49.5 | |

**Table 8 – 4457 Measured Compression Set, %**

| Weeks | 20% CPK-0 | 50% CPK-0 | 80% CPK-0 | 100% CPK-0 | Jet A_16 | Jet A_16 | CPK-0 |
|---|---|---|---|---|---|---|---|
| 0 | 0.0 | 0.0 | 0.0 | 0.0 | 0.0 | 0.0 | 0.0 |
| 2 | 26.4 | 23.9 | 19.6 | 18.2 | 19.1 | 16.0 | |
| 4 | 31.1 | 28.5 | 24.2 | 22.7 | 23.1 | | 21.0 |
| 6 | 34.4 | 31.2 | 27.3 | 25.8 | 27.1 | 23.1 | |
| 8 | 36.8 | 33.6 | 29.5 | 29.0 | 29.1 | | 25.5 |
| 10 | 39.2 | 35.9 | 31.3 | 30.6 | 31.6 | 27.4 | |
| 12 | 41.2 | 38.6 | 33.5 | 32.7 | 33.4 | | 29.9 |
| 14 | 43.4 | 39.7 | 35.4 | 34.4 | 36.5 | 31.7 | |
| 16 | 45.9 | 42.0 | 37.6 | 36.4 | 39.9 | | 34.2 |
| 18 | 47.3 | 43.8 | 40.0 | 38.3 | 41.9 | 35.7 | |
| 20 | 49.9 | 45.7 | 41.4 | 40.7 | 43.1 | | 38.3 |
| 22 | 50.8 | 47.3 | 42.3 | 43.1 | 45.9 | 39.4 | |
| 24 | 51.9 | 48.5 | 43.6 | 44.1 | 47.9 | | 42.0 |
| 26 | 53.5 | 49.9 | 45.7 | 45.6 | 50.3 | 43.0 | |

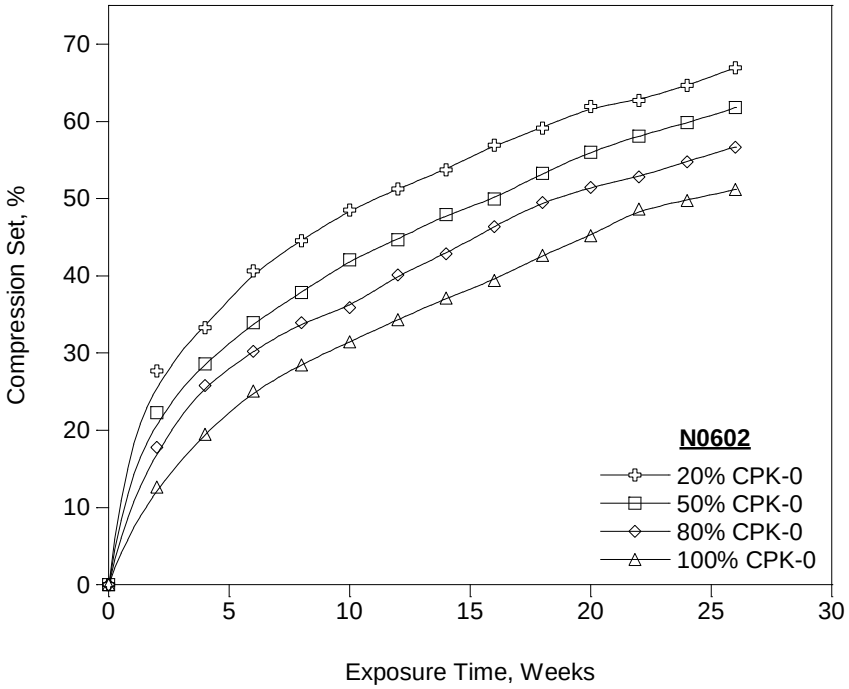


**Figure 8. The average compression set of the N0602 O-rings in the test fuels.**

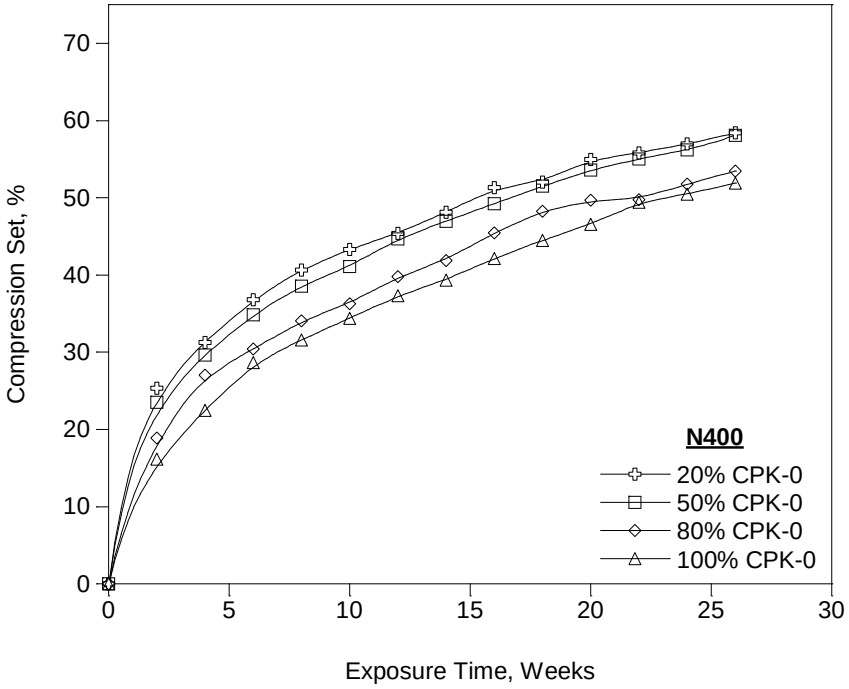


**Figure 9. The average compression set of the N400 O-rings in the test fuels.**

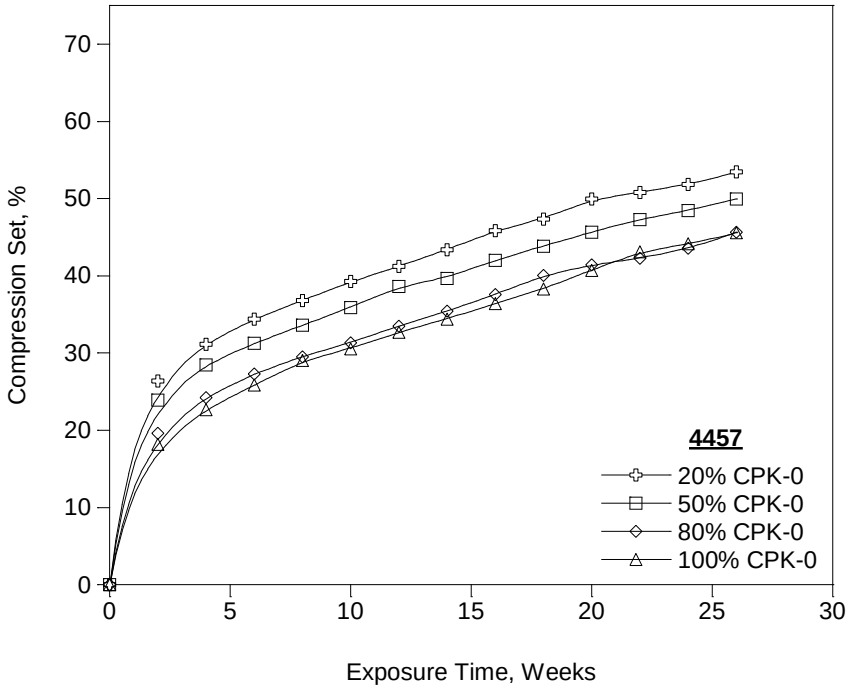


**Figure 10. The average compression set of the 4457 O-rings in the test fuels.**

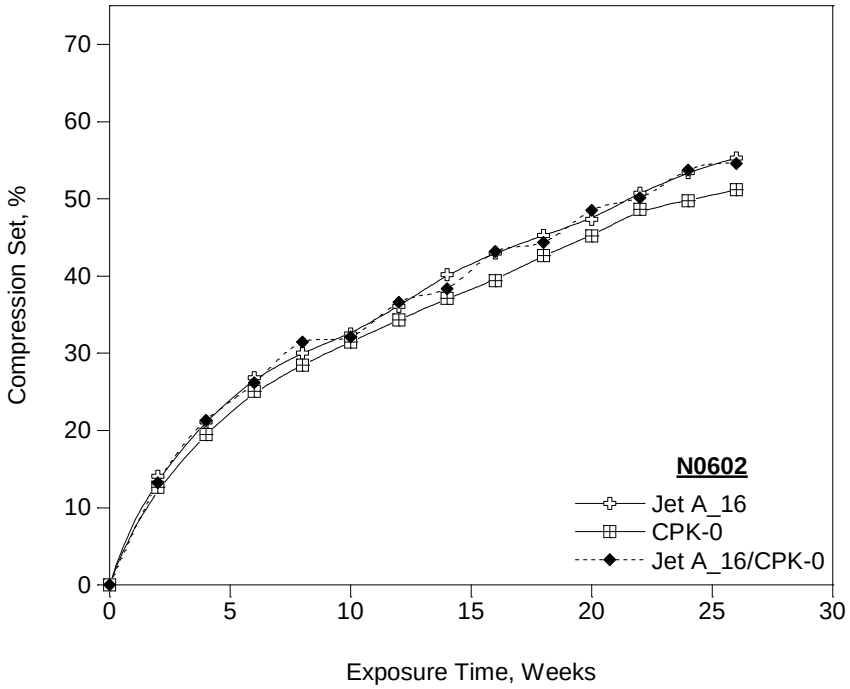


**Figure 11. Compression set as a function of time for N0602 O-rings when exposed to a single fuel (Jet A_16 or CPK-0) and periodically switched between Jet A_16 and CPK-0. Note that the switch-load data points are joined using a cubic spline fit and this curve may not reflect the true temporal behavior.**

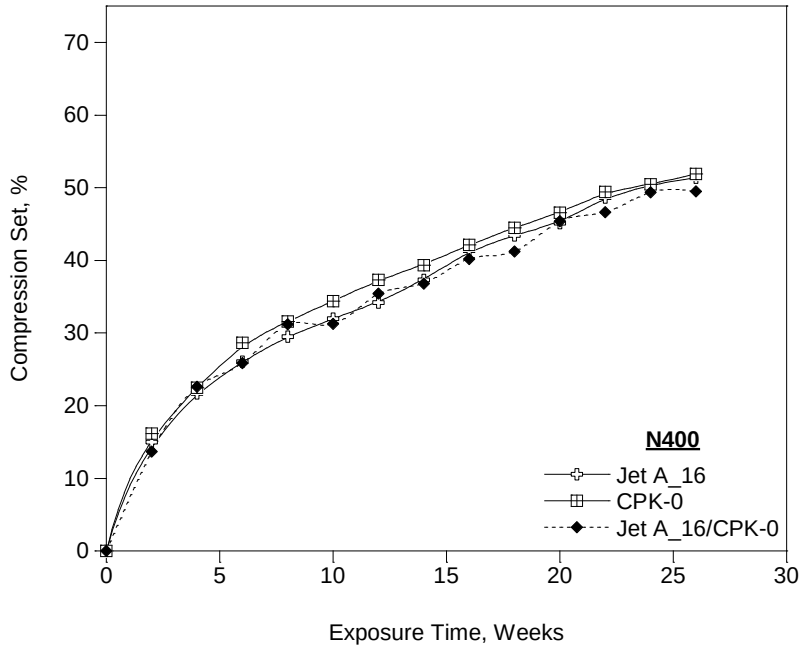


**Figure 12. Compression set as a function of time for N400 O-rings when exposed to a single fuel (Jet A_16 or CPK-0) and periodically switched between Jet A_16 and CPK-0. Note that the switch-load data points are joined using a cubic spline fit and this curve may not reflect the true temporal behavior.**

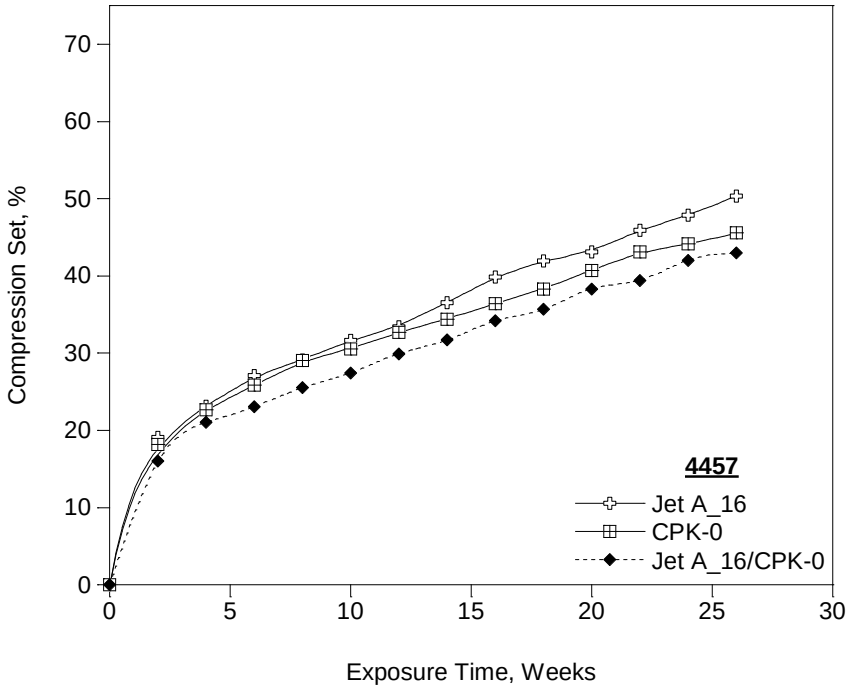


**Figure 13. Compression set as a function of time for 4457 O-rings when exposed to a single fuel (Jet A_16 or CPK-0) and periodically switched between Jet A_16 and CPK-0. Note that the switch-load data points are joined using a cubic spline fit and this curve may not reflect the true temporal behavior.**

### *Post-Run Physical Properties*

After the completion of the compression set evaluation selected physical properties were measured as summarized in Table 9. To condition the O-rings into a common state the test pieces were removed from their respective test fuels, dabbed dry with a laboratory tissue, and placed in Jet A_16 for 1 week at room temperature. The O-rings were then removed from the Jet A_16, dabbed dry, and placed in a fresh volume of Jet A_16 for an additional week. The test pieces were stored in Jet A_16 until their post-run testing was conducted.

**Table 9 – Task 4 Post-Run Set Tests**

| Property | Method | Notes |
|---|---|---|
| Hardness, Type M | ASTM D2240 | Shore M |
| Tensile | ASTM D1414 | Tensile Strength |
| Elongation | ASTM D1414 | Ultimate Elongation |
| Modulus at 100% Elongation | ASTM D1414 | Concurrent with ASTM D1414 |
| IR Spectrum | ATR | Attenuated Total Reflectance |
| Glass Transition | ASTM E1545 | Thermomechanical Analysis |

### *Hardness*

The type M hardness test results are summarized in Table 10 and Figure 14. Note that these results include the baseline results for the dry O-rings as evaluated in Task 1. These show that the hardness of the N400 O-rings was relatively constant across Tasks 1-3 while the hardness of the N0602 and 4457 O-rings increased slightly as compared to the baseline Task 1 possibly as a consequence of the extraction of plasticizer by the test fluids and the subsequent absorption of the test fluid which only partially replaces the lubricating function of the original plasticizer. Note that the Jet A_16/CPK-0 fuel switching did not have a significant effect on the final hardness of the test pieces as compared to the exposures in the various SPK/CPK-0 blends.

**Table 10 – Type M Hardness**

| Fluid | Hardness, Type M | | |
|---|---|---|---|
| | N0602 | N400 | 4457 |
| None (Task 1) | 77 | 79 | 77 |
| 20% CPK-0 | 82 | 79 | 80 |
| 50% CPK-0 | 80 | 78 | 80 |
| 80% CPK-0 | 79 | 78 | 80 |
| 100% CPK-0 | 80 | 79 | 80 |
| Jet A_16/CPK-0 (Switch Loading) | 81 | 79 | 81 |

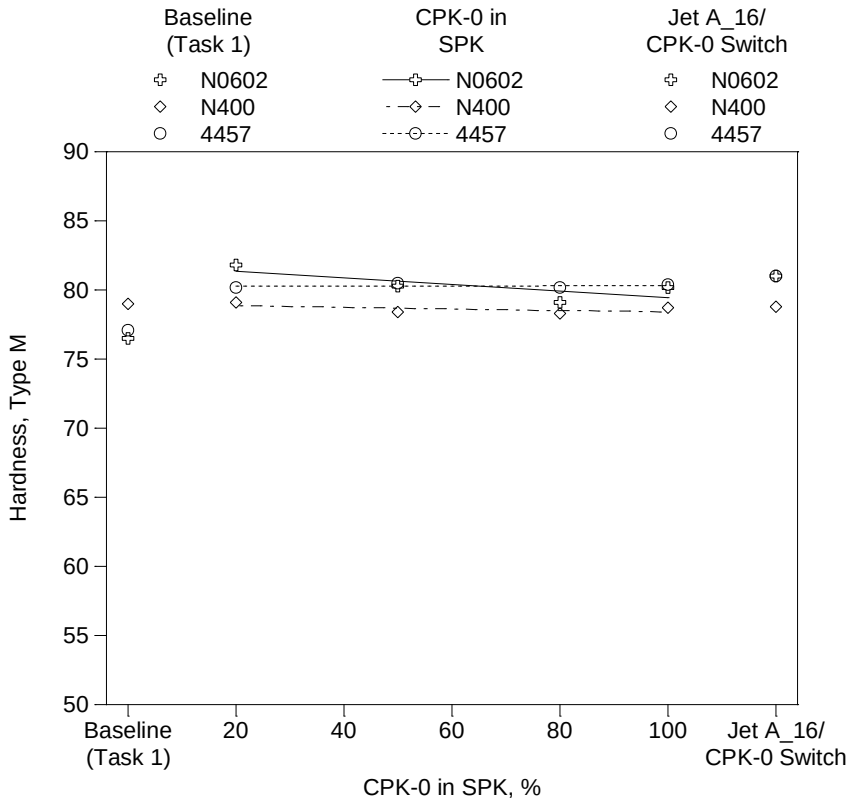


**Figure 14. Summary of the post-compression set Type M hardness.**

***Tensile***

The tensile test results are summarized in Table 11 and Figure 15. Note that these results include the baseline results for the dry O-rings as evaluated in Task 1. These show that the tensile of the test O-rings decreased slightly as compared to the baseline Task 1 possibly as a consequence of the extraction of plasticizer by the test fluids and the subsequent absorption of the test fluid which only partially replaces the lubricating function of the original plasticizer. Note that the Jet A_16/CPK-0 fuel switching did not have a significant effect on the final tensile of the test pieces as compared to the exposures in the various SPK/CPK-0 blends.

**Table 11 – Tensile**

| Fluid | Tensile, psi | | |
|---|---|---|---|
| | **N0602** | **N400** | **4457** |
| None (Task 1) | 1757 | 1937 | 1429 |
| 20% CPK-0 | 1436 | 1412 | 1242 |
| 50% CPK-0 | 1483 | 1451 | 1272 |
| 80% CPK-0 | 1486 | 1578 | 1300 |
| 100% CPK-0 | 1637 | 1642 | 1199 |
| Jet A_16/CPK-0 | 1417 | 1653 | 1264 |

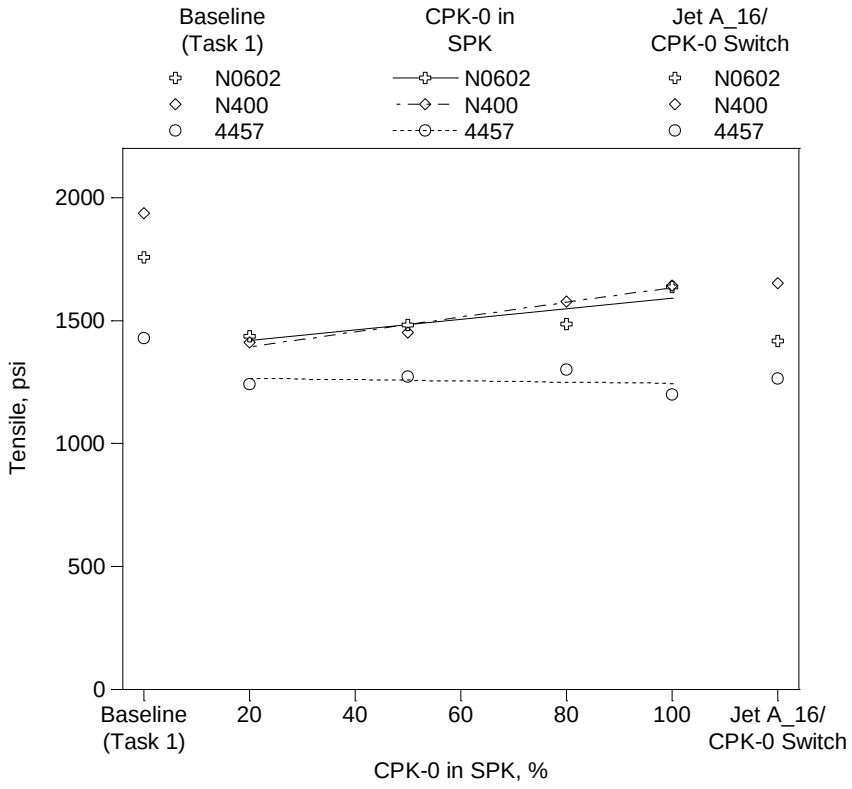


**Figure 15. Summary of the post-compression set tensile.**

***Elongation***

The elongation test results are summarized in Table 12 and Figure 16. Note that these results include the baseline results for the dry O-rings as evaluated in Task 1. In a manner similar to the tensile reported above, the elongation of the test O-rings decreased as compared to the baseline Task 1 possibly as a consequence of the extraction of plasticizer by the test fluids and the subsequent absorption of the test fluid which only partially replaces the lubricating function of the original plasticizer. In contrast, the elongation showed only a slight change as a function of the CPK-0 concentration in SPK as tested in this task. Note that the Jet A_16/CPK-0 fuel switching did not have a significant effect on the final tensile of the test pieces as compared to the exposures in the various SPK/CPK-0 blends.

**Table 12 – Elongation**

| | Elongation, % | | |
|---|---|---|---|
| **Fluid** | **N0602** | **N400** | **4457** |
| None (Task 1) | 308 | 255 | 234 |
| 20% CPK-0 | 142 | 145 | 124 |
| 50% CPK-0 | 143 | 151 | 129 |
| 80% CPK-0 | 139 | 164 | 133 |
| 100% CPK-0 | 140 | 173 | 125 |
| Jet A_16/CPK-0 | 134 | 171 | 129 |

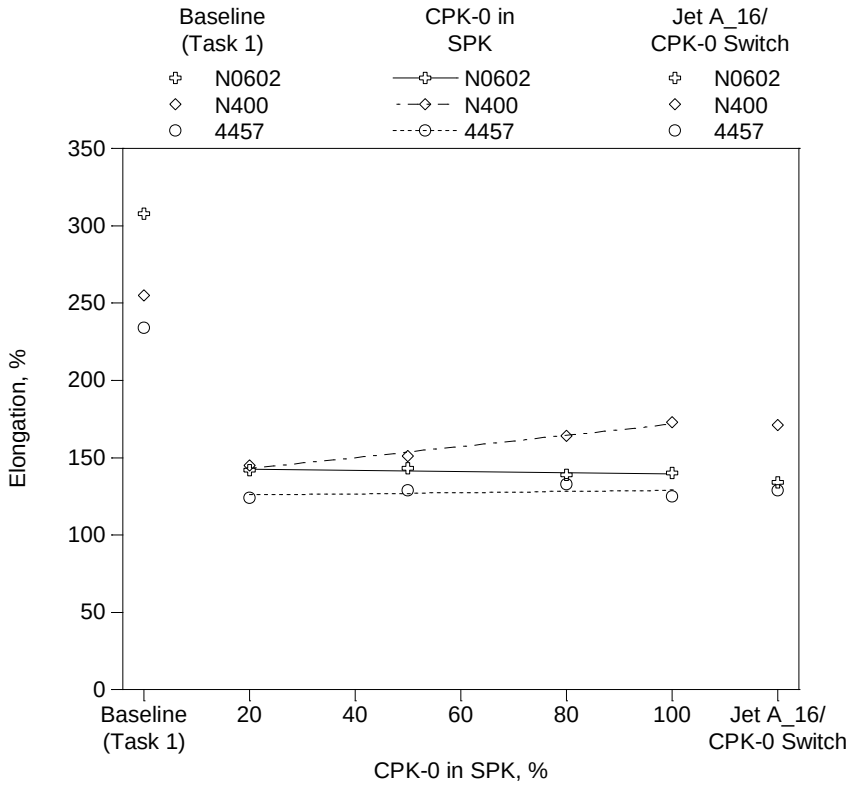


**Figure 16. Summary of the post-compression set elongation.**

***Modulus at 100% Elongation***

The modulus at 100% elongation, M(100), test results are summarized in Table 13 and Figure 17. Note that the O-rings from Task 1 were the dry source O-rings. These results show that the M(100) of the test O-rings from Task 4 were higher than the source O-rings in a manner similar to that observed from Tasks 2 and 3. This may be a consequence of the extraction of the plasticizer by the test fuels and the absorption of components from the test fuel by the O-rings. Within the bounds of Task 4 the data shows a slight increase in the M(100) of the N0602 as the concentration of CPK-0 increased in the test fuels while the M(100) for the N400 and 4457 was unchanged or slightly decreased. The M(100) from the Jet A_16/CPK-0 switch-load compared well with the average values from the single fuel exposures suggesting that the switch-loading did not have a significant effect on the physical properties of the elastomers.

**Table 13 – Modulus at 100% Elongation**

| Source | Modulus at 100% Elongation | | |
|---|---|---|---|
| | N0602 | N400 | 4457 |
| None (Task 1)* | 474 | 728 | 680 |
| 20% CPK-0 | 1220 | 1168 | 1123 |
| 50% CPK-0 | 1254 | 1101 | 1085 |
| 80% CPK-0 | 1301 | 1116 | 1088 |
| 100% CPK-0 | 1381 | 1132 | 1019 |
| Jet A_16/CPK-0 | 1283 | 1133 | 1047 |

*As-received, no conditioning

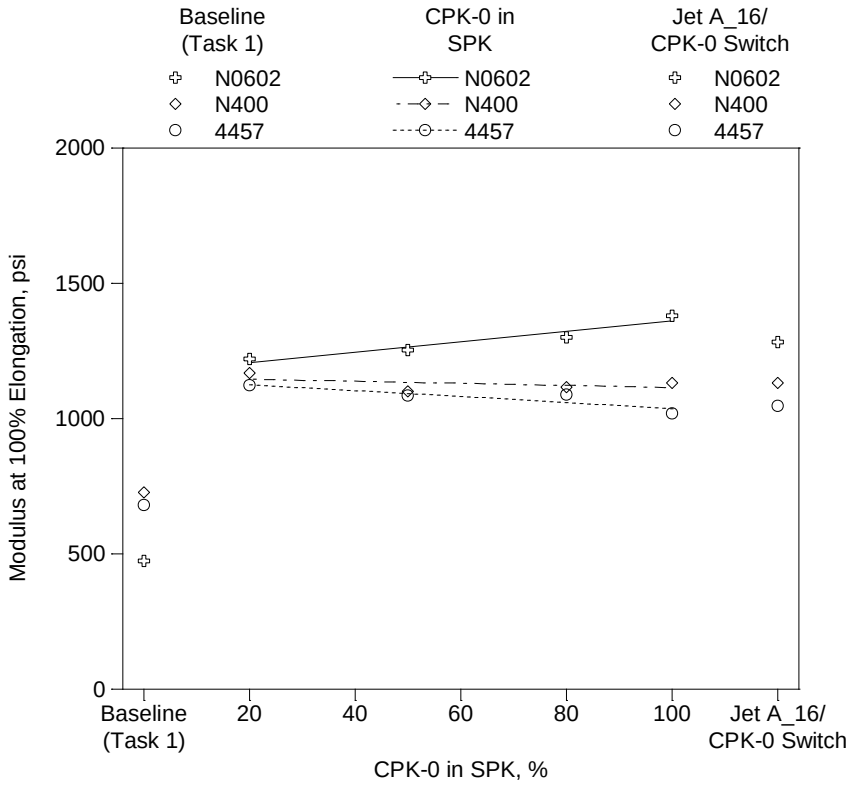


**Figure 17. Summary of the post-compression set modulus at 100% elongation.**

***Glass Transition Temperature, Tg***

The glass transition temperature (Tg) of the source, as-received O-ring materials (no conditioning) and the test O-rings from Task 4 after being conditioned in Jet A_16 are summarized in Table 14 and Figure 18. These results show how the Tg increased slightly as the level of CPK-0 increased and after the Jet A_16/CPK-0 switch-loading. This may reflect the removal of the plasticizer from the O-rings becoming more efficient as the solvent character of the test fluid increases with the increasing level of CPK-0 in the SPK as tested here.

**Table 14 – Glass Transition Temperature of the Test O-rings Conditioned in Jet A_16**

| Fluid | Tg, C | | |
|---|---|---|---|
| | N0602 | N400 | 4457 |
| None (Task 1)* | -51.2 | -49.5 | -50.8 |
| 20% CPK-0 | -49.8 | -51.9 | -46.9 |
| 50% CPK-0 | -52.2 | -50.4 | -48.7 |
| 80% CPK-0 | -47.1 | -49.1 | -45.1 |
| 100% CPK-0 | -48.2 | -46.7 | -45.5 |
| Jet A_16/CPK-0 | -47.8 | -46.8 | -45.1 |

*As-received, no conditioning

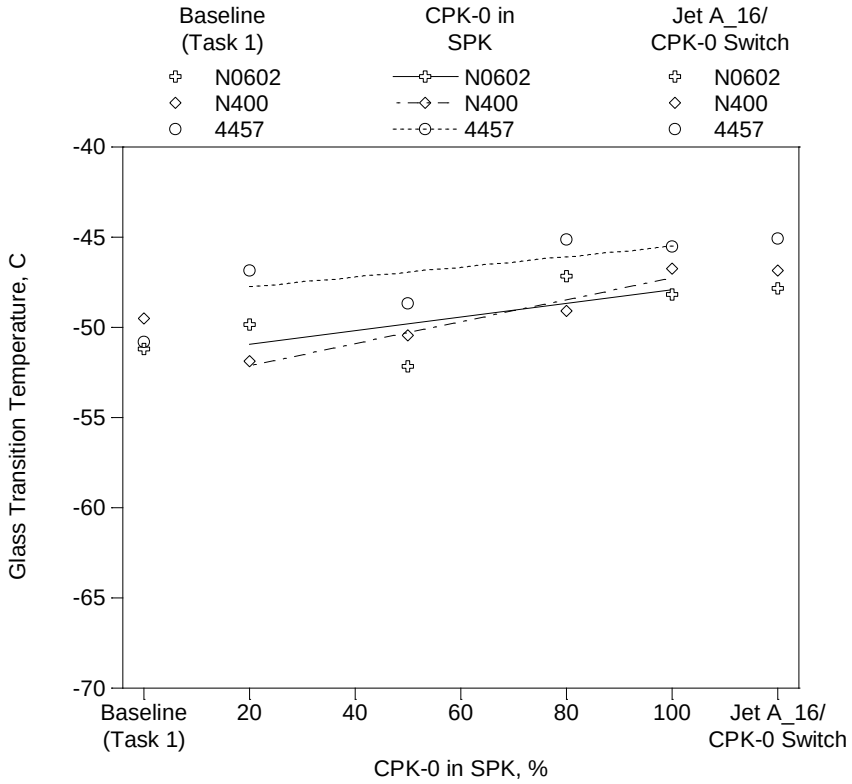


**Figure 18. Summary of the post-compression set glass transition temperature.**

### *Infrared Spectra*

Infrared spectra were obtained for the source and test O-rings using a Fourier-transform infrared spectroscopy using a diamond micro-ATR crystal sampling technique in a manner similar to that used in Task 1. Samples were prepared as O-rings cross sections that were extracted with methylene chloride and dried to remove the absorbed fuel (and plasticizer from the source samples) and to condition the samples to a common state. Spectra were obtained from the cut face of each sample to access the cleanest possible elastomer in the bulk sample. The results are summarized in Figure 19. Overall, these show that the IR spectra from each sample is very similar. Unfortunately, these data do not show a clear absorption feature at ~2250 $cm^{-1}$ that is characteristic of the –CN group, reflecting the challenge associated with

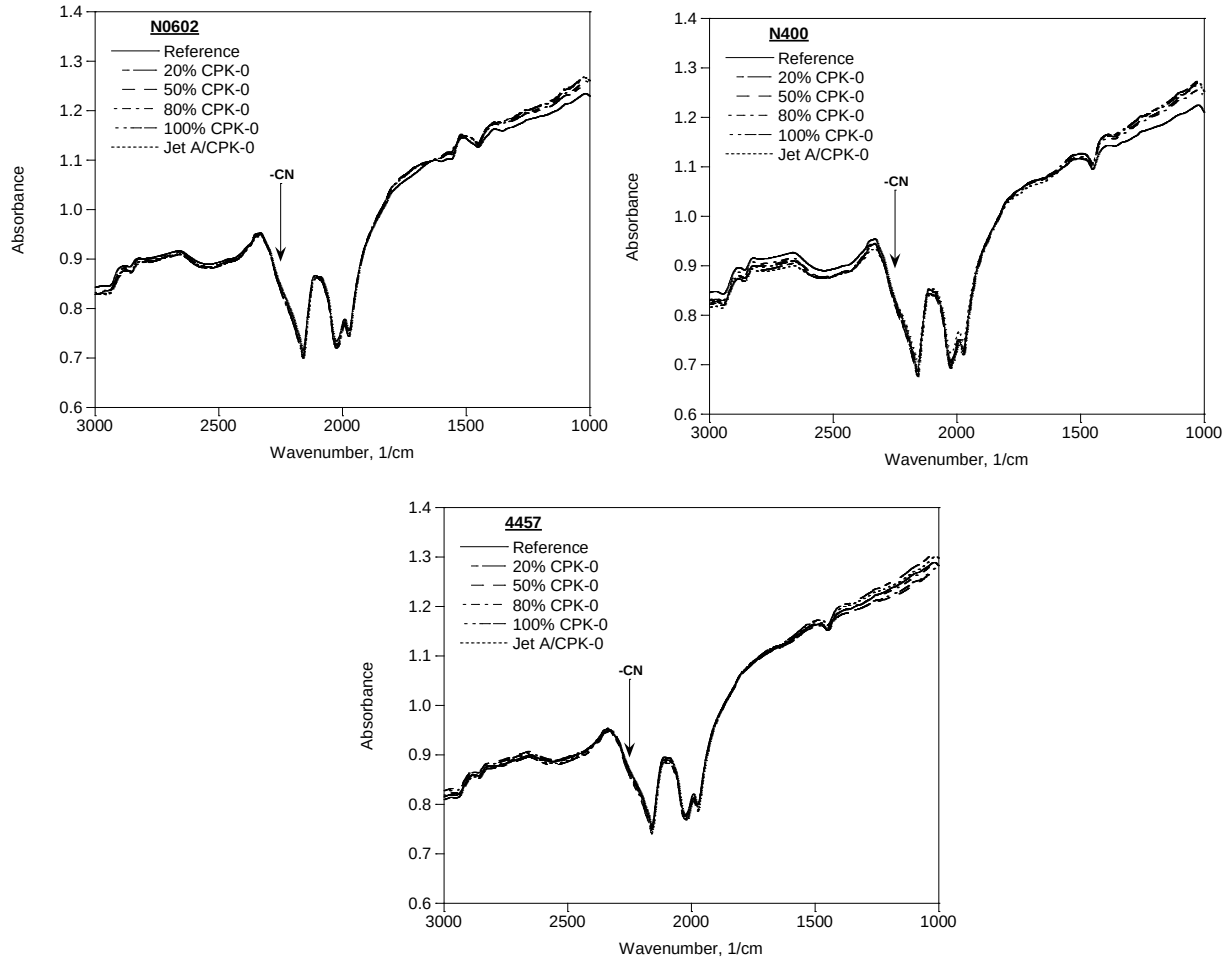


**Figure 19. Summary of the post-compression set IR spectra of the O-ring materials after being extracted and dried along with the spectra of the source materials. The expected absorption region for the –CN group (~2250 $cm^{-1}$) is indicated.**

carbon black. However, these spectra suggest that the exposure to the different fuels had little, if any, effect on the bulk composition of the elastomer. Note that in the initial evaluation reported in Task 1 a germanium micro-ATR crystal was used and the analysis proved problematic, likely due to the high carbon black loading of the elastomer. Subsequent evaluations were conducted with a diamond crystal, though as reported above this analysis remained challenging. An initial investigation using pyrolysis GC-MS to evaluate the acrylonitrile content of nitrile was encouraging and this approach may be considered in any future work.

### Task 5 - Optical Cell Leak Testing

At the conclusion of Task 2, two O-rings from each fuel were set aside and stored in their respective test fuels for additional testing using an optical flow cell illustrated in Figure 20. This test fixture consists of a nominal face seal designed to provide up to 30% compression with an internally pressurized size 214 O-ring. The top plate of this fixture consists of a ½" thick glass window that provides optical access to the O-ring during the test. Fuel is delivered to the inside

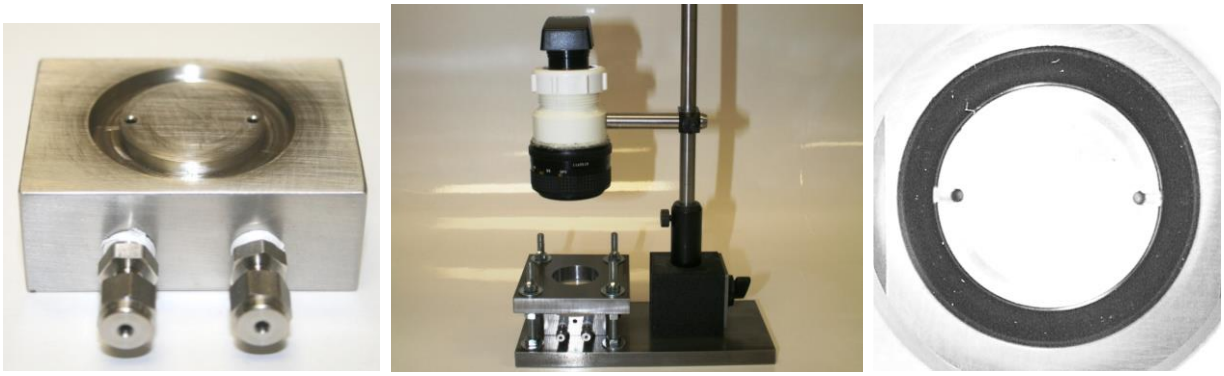

Compression Flow Cell | Compression Fixture Configured For Optical Access | Example O-ring Image @ 60 psi

**Figure 20. The UDRI flow cell (left) configured with a glass top plate for optical access (middle) with an example image of an O-ring pressurized to 60 psi (right).**

diameter of the O-ring as it would be in service and pressurized with a blow-down fuel tank. For each evaluation the test O-ring is removed from the previous test fuel, dabbed dry, installed in the optical fixture, compressed 25%, and then photographed to record the visual appearance of the O-ring and the dimensions of the contact band between the O-ring and the faces of the seal. Fuel is then purged through the cell to flush the air from the system and to fill the gland with fluid. The flow is then reduced using a metering valve located downstream of the flow cell so that the pressure in the cell is essentially the same as in the blow-down tank. The O-ring is allowed to condition for 5 minutes, inspected for leaks, and photographed. The pressure in the blow-down tank is then set to the next test point and the process repeated. For this program the test O-ring was initially conditioned at 5 psi, and then tested at 10, 20, 30, 40, 50, and 60 psi.

***Estimating the Sealing Pressure of the Task 2 O-rings***

While the optical flow cell is useful in determining whether an O-ring will leak under the conditions of the test, it does not provide information on the sealing pressure (force per unit area) being applied by the O-rings itself against the faces of the seal. For example, in its current configuration the optical leak cell was designed to operate at pressures up to 60 psi. However, if the test piece does not leak at 60 psi, the actual sealing pressure is unknown. Alternatively, the optical flow cell can be used in conjunction with an Elastocon compressive stress relaxometer (CSR) to estimate the sealing pressure of the test O-ring. For this analysis the flow cell was mounted in the CSR as shown in Figure 21. As in the optical flow cell, the O-ring is compressed 25% and supplied with fuel flowing at essentially zero pressure. The sealing force is then measured with a load cell incorporated into the compression frame. To calculate the sealing pressure, the sealing force provided by the CSR is divided by the area of the O-ring contact band as measured by the optical flow cell.

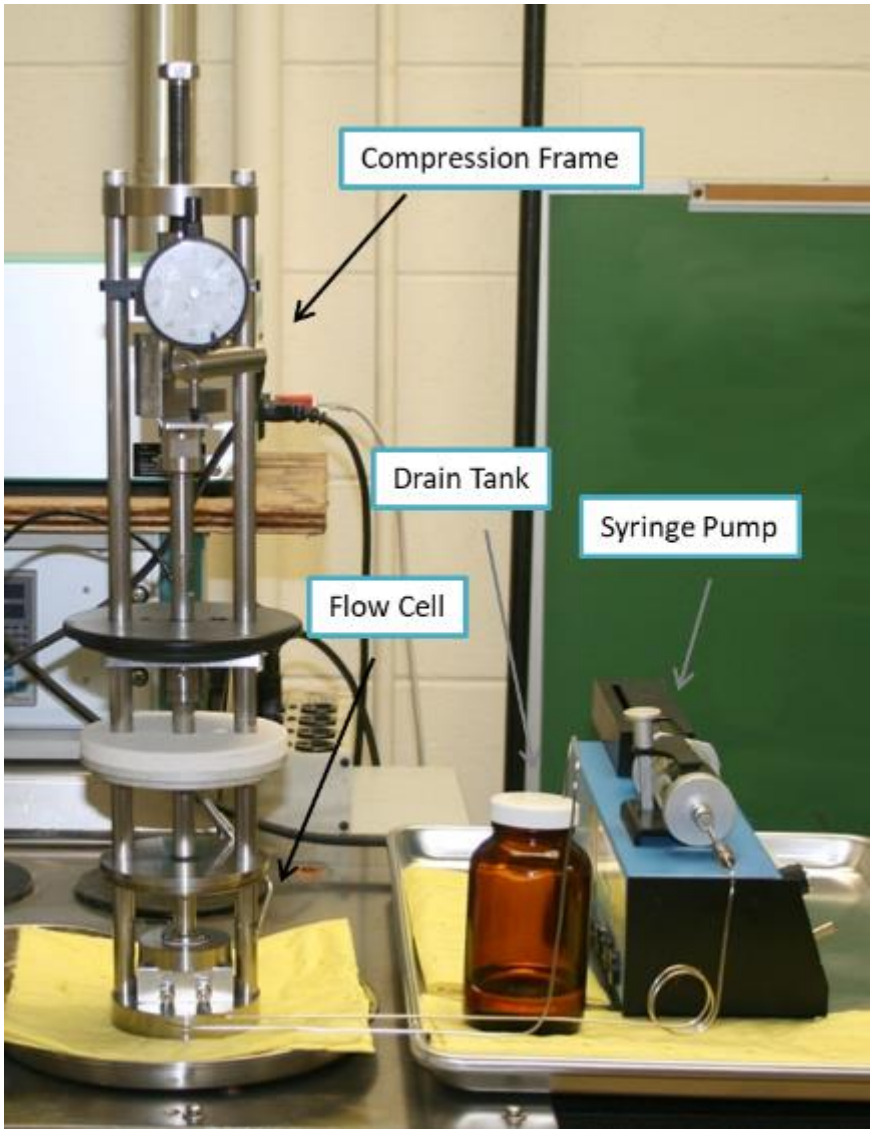


**Figure 21. The UDRI flow cell installed in an Elastocon compressive stress relaxometer.**

***The Effect of Fuel Composition on the Task 2 O-ring Dimensions***

While installing the test O-rings in the optical flow cell it was noted that the test pieces that were aged in Jet A_4 easily dropped in the O-ring gland, while the O-rings aged in Jet A_16 and Jet A_25 had swollen so much that they no longer fit into the gland as shown in Figure 22. This illustrates that when these O-ring swell in jet fuel they not only swell in the direction of compression, increasing the effective compression of the seal, they also swell in their overall dimensions, essentially making them over-sized for the gland for which they were designed to fit.

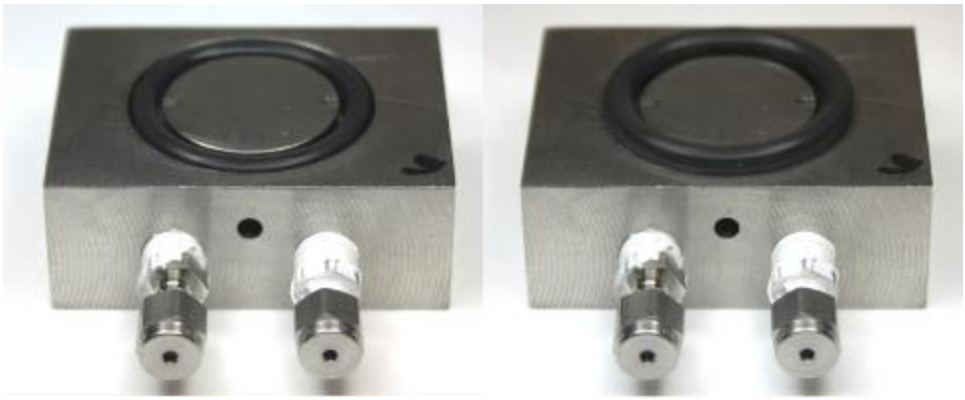


**Figure 22. An O-ring flow cell with an O-ring aged in Jet A_4 (left) and Jet A_25 (right) showing how the swollen O-ring no longer fits into the gland.**

To quantify the overall dimensions of the test O-rings, each of the test pieces were removed from their respective fuels, dabbed dry, and photographed as shown in Figure 23. From these photographs the dimensions of the O-rings were obtained and compared with original dimensions as specified by the manufacturer as shown in Figure 24. (Note that the dimensions in the compressed direction were measured using a micrometer.) These results illustrate how the linear dimensions increase as the aromatic content of the test fuels increases. Interestingly, with the exception of the axial cross section (the direction of compression), the dimensions of the O-rings aged in the low aromatic fuel (Jet A_4) are closer to the nominal dimensions of the source O-rings than are the swollen O-rings. The loss of cross section in the axial direction being the result of compression set. This suggests that one consequence of the O-ring swelling while in service is not just an increase in the compression diameter, but also an increase in the overall O-ring dimensions, essentially making the O-ring over-sized as compared to the original as-received and as-installed O-rings.

***Sealing Pressure of the Task-2 O-rings***

Prior to conducting the pressurized leak test, the sealing pressure of the test O-rings were measured as described above. For comparison the sealing pressure of dry source O-rings was also measured. The visual appearance and dimensions of the contact bands are summarized in Figure 25 and 26 for the dry source O-rings and test O-rings, respectively. Overall, these images show that the contact bands appear to be in good condition and that the area of the contact bands of the test pieces appear to increase with the aromatic content of the test fuels. The measured area of the contact bands along with the measured sealing force and resulting sealing pressure are summarized in Table 15 and Figures 27, 28, and 29 for the N0602, N400, and 4457, respectively. These show that the area of the contact band does increase with aromatic content, though the area relative to the dry source O-ring is material-specific. For example, the area of the contact band for the N0602 is the same or larger than the dry source O-ring. The area of the contact band for the N400 is slightly smaller with the samples aged in Jet A_4, but larger when aged in the Jet A_16 and Jet A_25. The area of the contact band for the 4457 is smaller than the dry source O-ring in Jet A_4 and Jet A_16, and about the same size

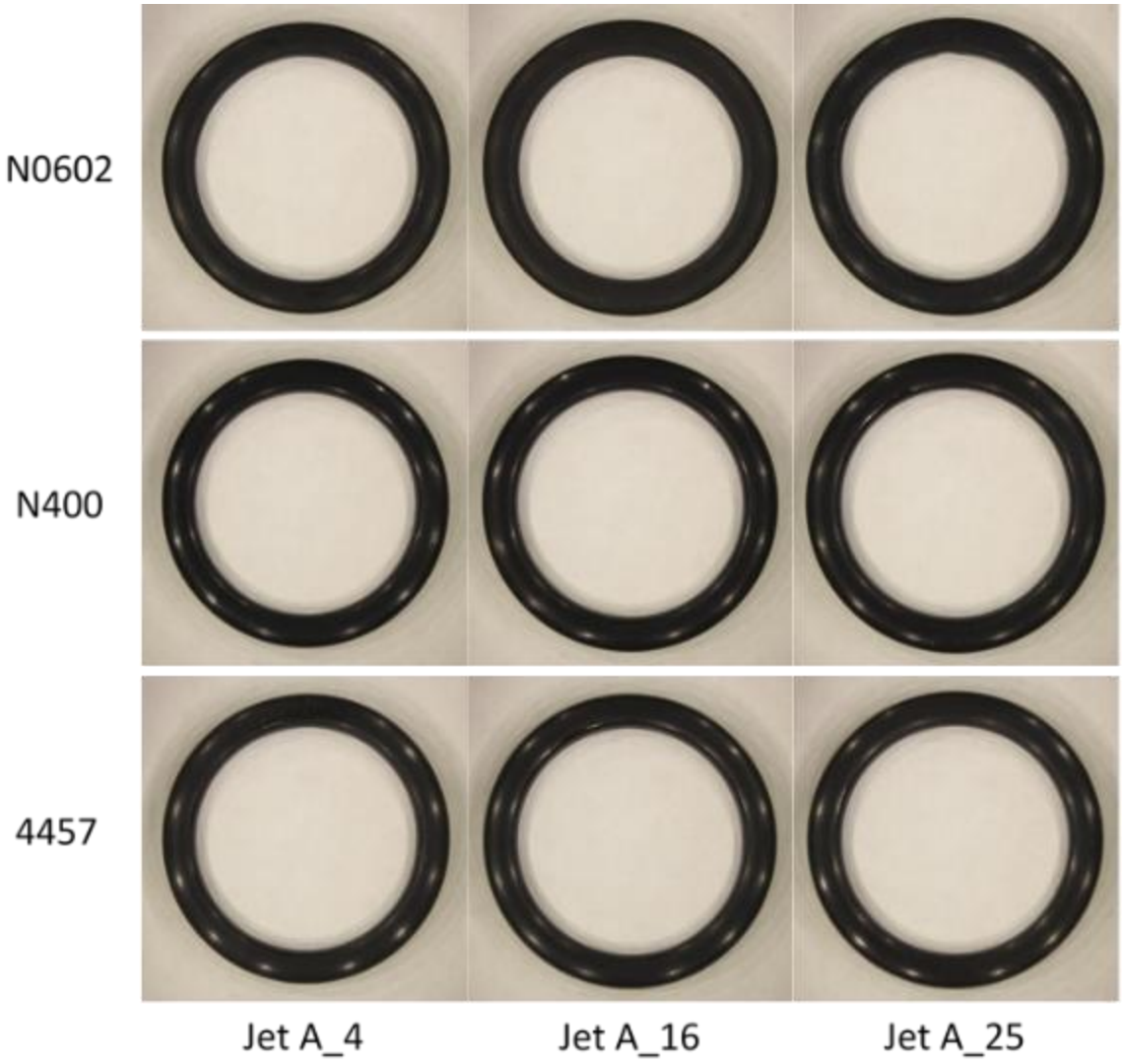


**Figure 23. Photographs of the test O-rings prior to being installed in the optical flow cell.**

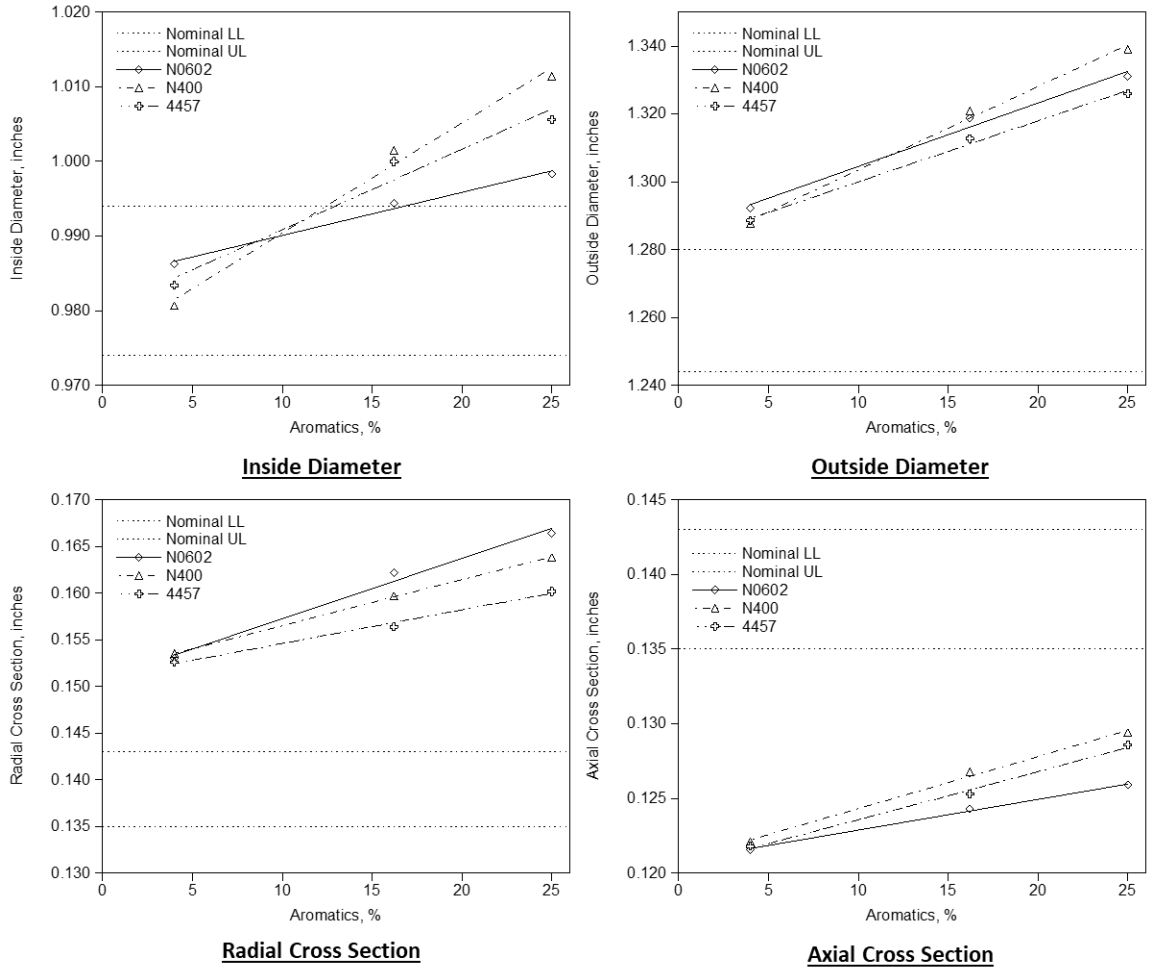


**Figure 24. Summary of the O-ring dimensions.**

when aged in Jet A_25. Similarly, the sealing force in all of the test O-rings increases with the aromatic content of the test fuel, though overall the sealing force of the test O-rings tends to be lower than with the dry source O-rings. This is likely a consequence of the O-rings softening and taking a set during the aging in fuel. Interestingly, the area of the contact band and the sealing force for the N0602 offset each other, giving a sealing pressure that is not a strong function of the aromatic content of the fuel for this material. In contrast, the sealing pressure of the N400 is a relatively strong function of the fuel composition, while the sealing pressure of the 4457 is a relatively modest function of the fuel composition. Note that the lowest sealing pressure measured for each of the test O-rings is significantly higher than the 60 psi used with the optical leak check and therefore none of these O-ring would be expected to leak when pressurized to 60 psi.

**Table 15 – O-ring Sealing Pressures**

| O-ring | Fuel | Area in^2 | Force N | Pressure psi |
|---|---|---|---|---|
| N0602 | None | 0.304 | 94.8 | 312 |
| | Jet A_4 | 0.306 | 42.8 | 140 |
| | Jet A_16 | 0.379 | 62.8 | 166 |
| | Jet A_25 | 0.424 | 59.1 | 140 |
| N400 | None | 0.330 | 97.8 | 296 |
| | Jet A_4 | 0.282 | 42.9 | 152 |
| | Jet A_16 | 0.373 | 79.4 | 213 |
| | Jet A_25 | 0.387 | 93.7 | 242 |
| 4457 | None | 0.347 | 97.1 | 280 |
| | Jet A_4 | 0.262 | 50.8 | 194 |
| | Jet A_16 | 0.334 | 62.0 | 186 |
| | Jet A_25 | 0.342 | 78.8 | 231 |

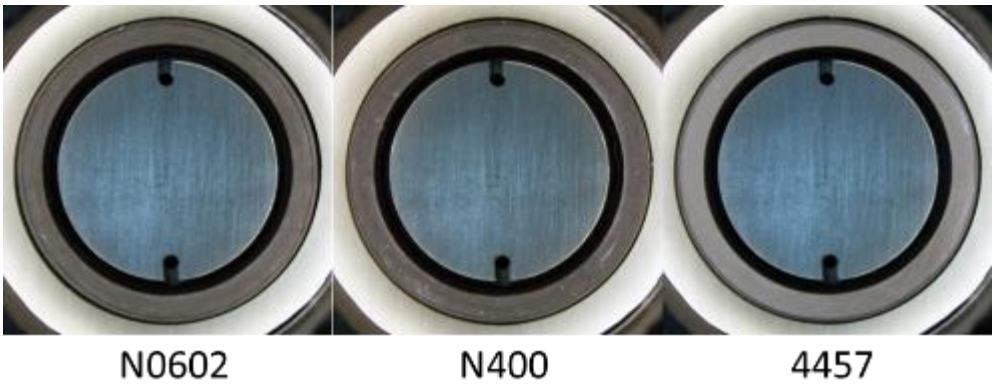


**Figure 25. Example images of the dry source O-rings compressed 25% in the optical flow cell.**

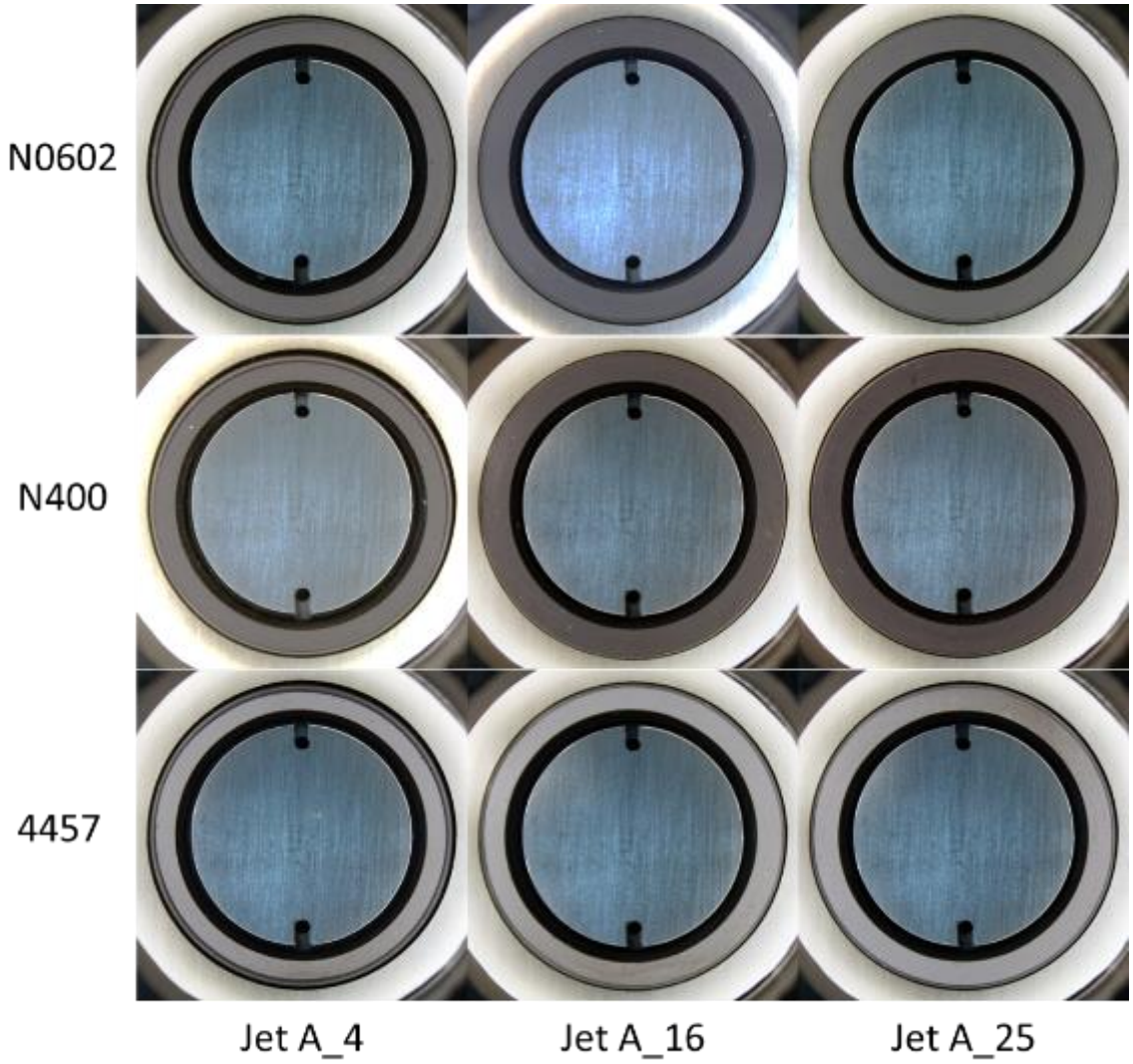


**Figure 26. Example images of the test O-rings compressed 25% in the optical flow cell.**

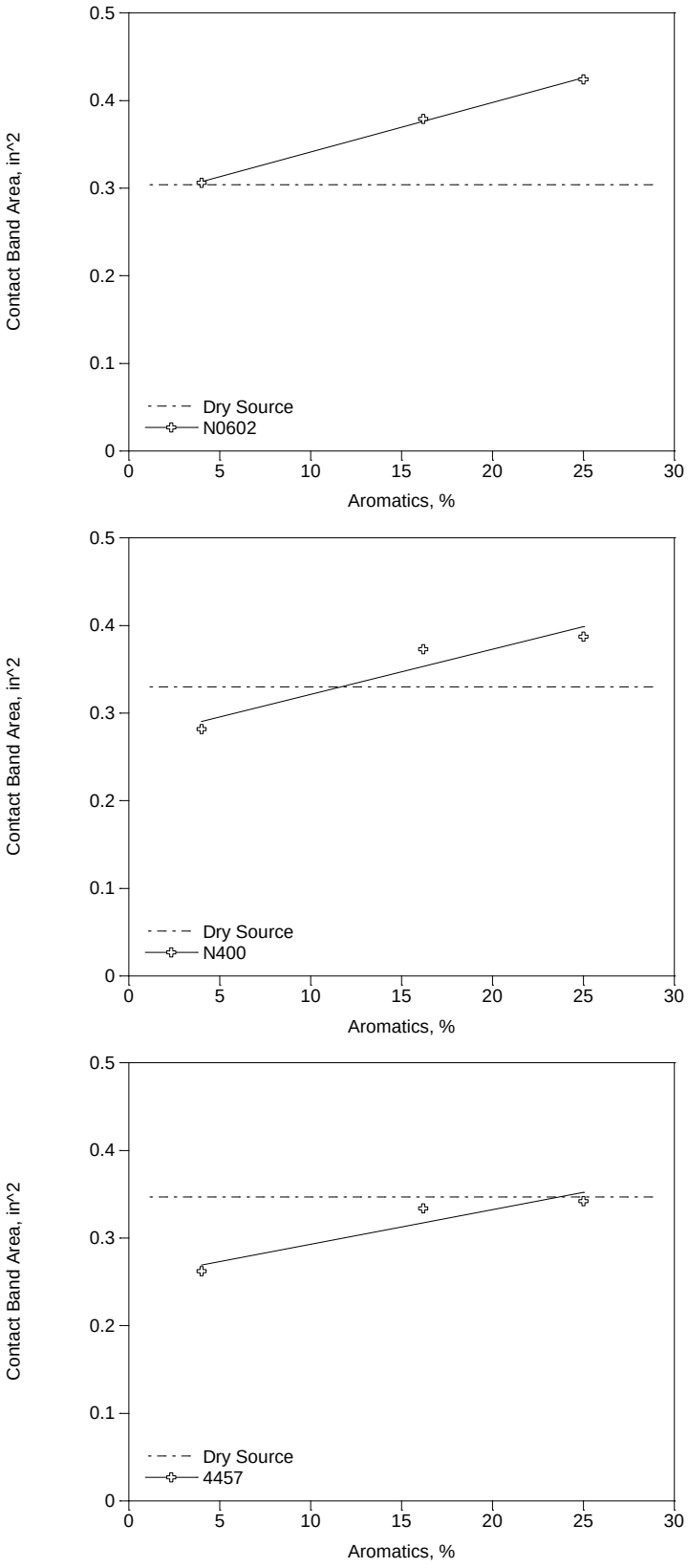


**Figure 27. Area of the O-ring contact bands.**

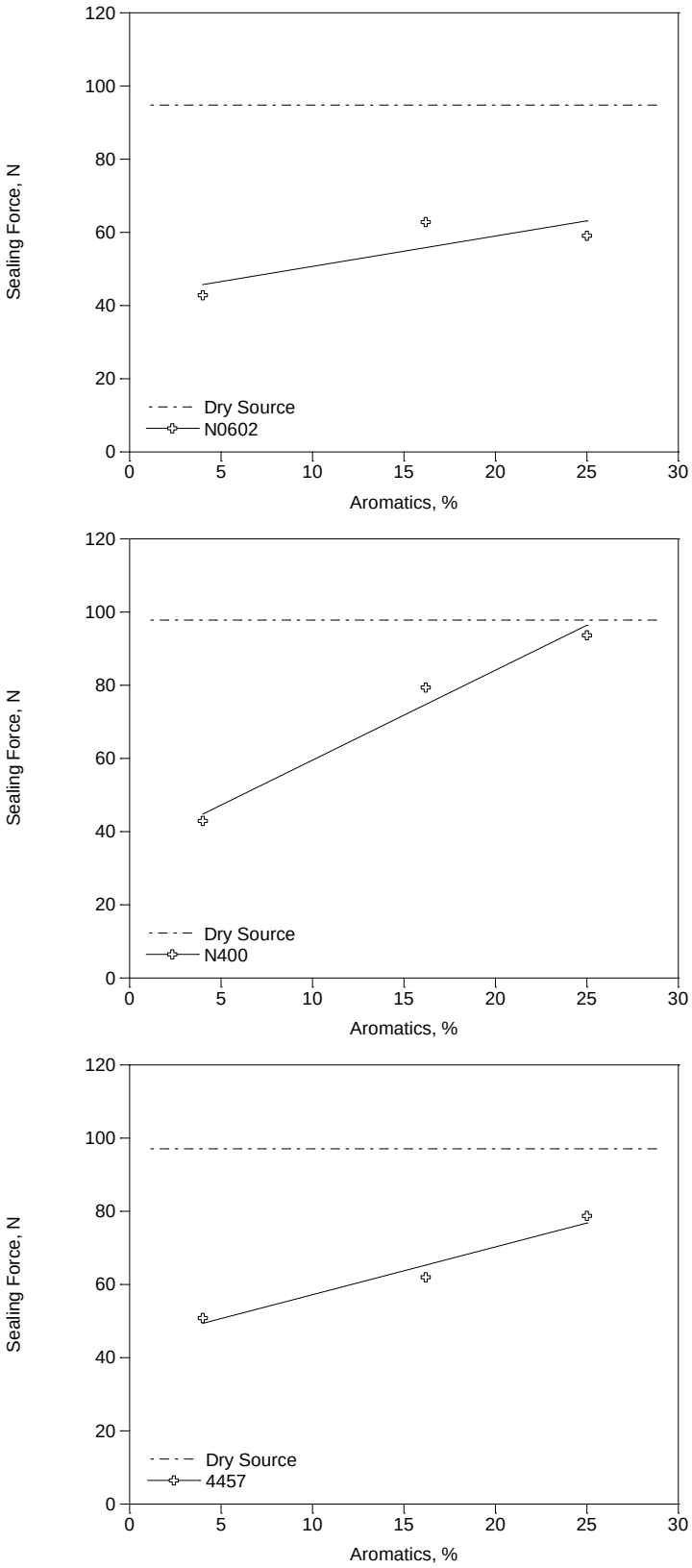


**Figure 28. O-ring sealing force.**

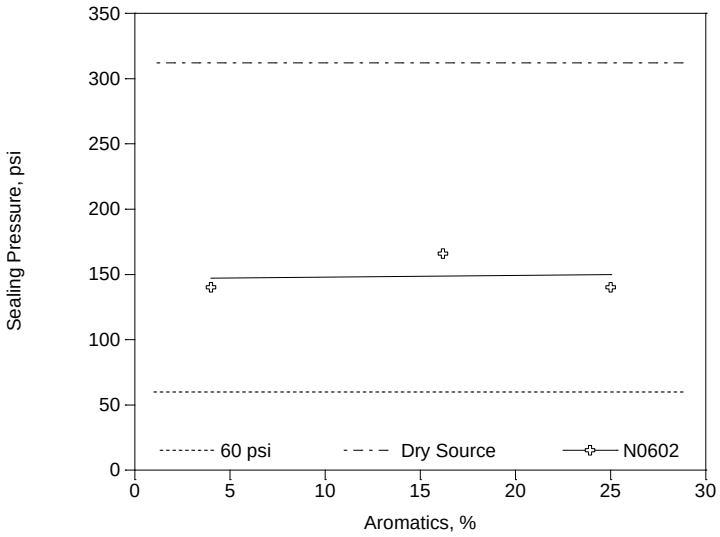


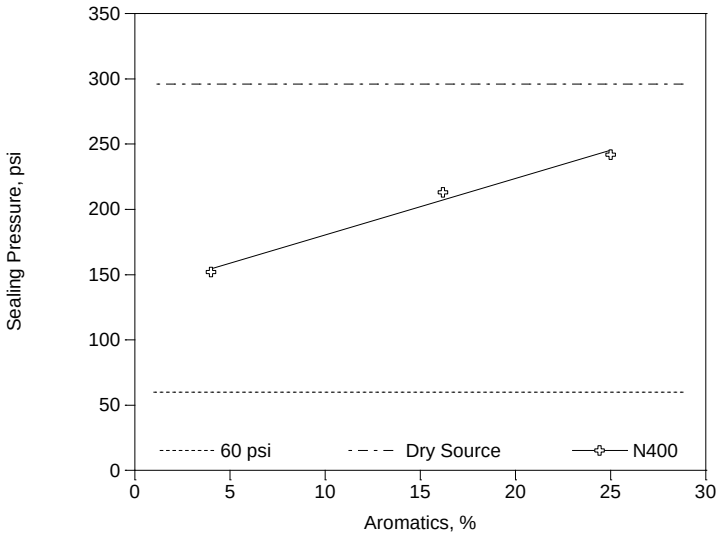


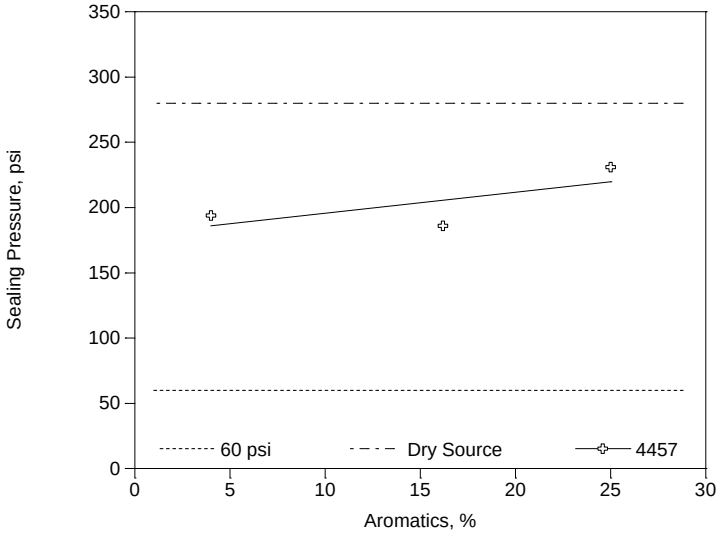


**Figure 29. O-ring sealing pressure.**

***Optical Leak Check of the Task 2 O-rings***

The original test plan in the technical proposal describes a process whereby the test O-rings would be tested in the optical flow cell at 60 psi to determine whether they will leak in each of the respective test fuels. The fuel would then be switched to an SPK fuel with 0% to 100% CPK-0 to observe the transition from leaking in the SPK to sealing in a SPK/CPK-0 blend. However, since the measured sealing pressure suggested that none of the test O-rings would leak in their respective test fuels and that it was unlikely that they would leak in 100% SPK, an abbreviated leak check was performed. For this evaluation, a leak check was performed only on the O-rings aged in Jet A_4 and subsequently conditioned in SPK. To observe the effect of switching the fuel from Jet A_4 to SPK the O-rings were conditioned in the Elastocon CSR as shown in Figure 21. One example of each O-ring aged in Task 2 with Jet A_4 was mounted in a flow cell, compressed 25%, and conditioned in Jet A_4 for approximately 18 hours (overnight) and then switched to SPK for approximately 72 hours at 30˚C. The relative sealing force of each of the test O-rings during this conditioning is given in Figure 30. This shows the typical initial rapid loss of sealing force as the O-ring relaxes in the gland. It is interesting to note that the switch from Jet A_4 to SPK had almost no effect on the rate of relaxation. This illustrates that the change from Jet A_4 to SPK is relatively small.

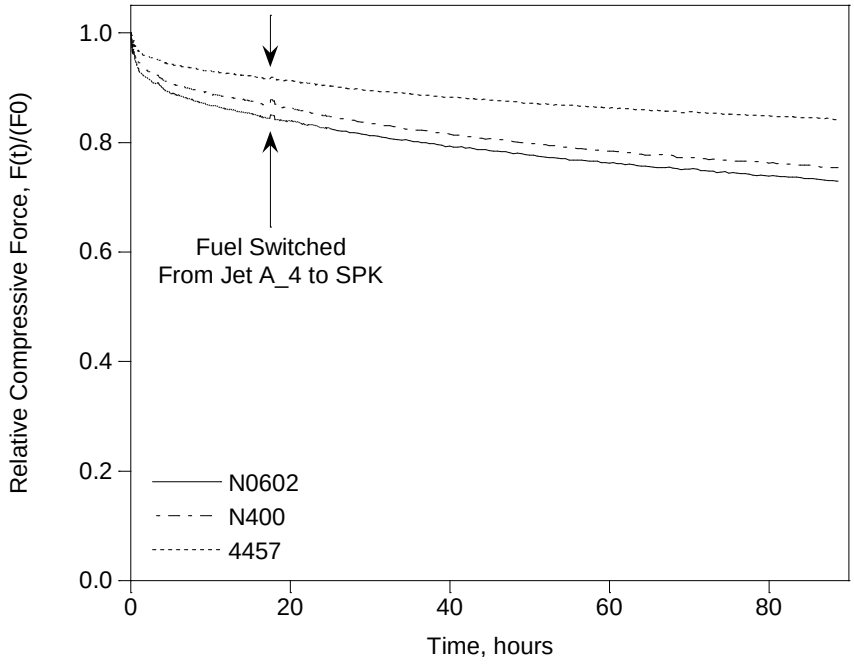


**Figure 30. The relative sealing force as a function of time during the conditions of the leak check O-rings.**

After the test O-rings were conditioned, they were removed from the Elastocon CSR, mounted in the optical leak cell and tested from 10 psi to 60 psi as described above. As expected, none of the O-rings developed leaks. Instead, the O-rings behaved as previously observed in similar tests. The observation is documented in Figure 31. Briefly, each O-ring provided a good seal at 10 psi. As the pressure increased, the O-ring expanded, pressing against the outside diameter of

the gland and likely increasing the compression against the face seal. In a manner similar to a check valve increasing the fluid pressure likely increases the sealing pressure and a leak will not develop even at higher pressures. Prior work with similar O-rings suggests that a leak will develop only when the condition of the contact band degrades to the point where the O-ring develops a leak before the fuel reaches sufficient pressure to compress the O-ring and initiates this check valve-like behavior. Consequently, as discussed below, the test O-rings were returned to their perspective test fuels in the compression set fixtures and aged at 160˚F until they reached a higher level of compression set.

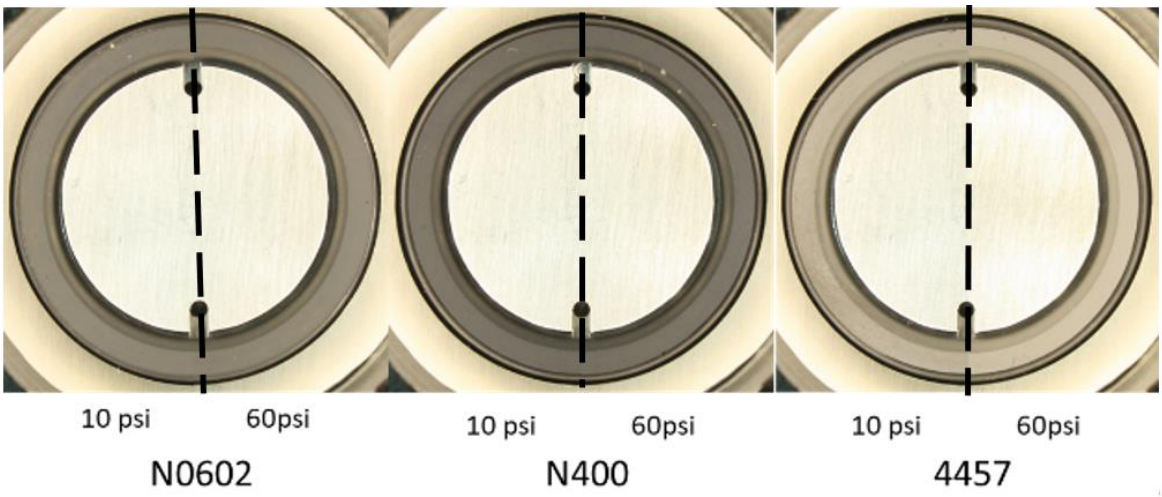


**Figure 31. Example leak check images showing the appearance of each O-ring at 10 psi (left half) and 60 psi (right half).**

***Additional Conditioning and Final Evaluation of the Task 2 O-rings***

To condition the O-rings from Task 2 to an advanced state of compression set, they were returned to the compression set fixtures and placed in their respective fuels at 160˚F. As before, every 2 weeks they were cooled to room temperature, removed from their fixtures, measured, and then returned to conditioning. The compression as a function of time from this extended conditioning is summarized in Table 16 and Figures 32, 33, and 34 for the N0602, N400, and 4457, respectively. Note that the O-rings were removed from the fixtures and were stored in their respective fuels for several weeks between Task 2 and Task 5 which allowed them to relax as shown by the discontinuity in the data. Note that the compression for all of the O-rings approached a limiting value and that the progressive loss of compression (accumulation of compression set) approached a limiting value suggesting that as the compressive stress is reduced it reaches a point where there is insufficient stress to energize chain slip and the loss of compression essentially comes to a halt. This may be a significant contributing factor for the relatively long service life of compression seals.

## Table 16 – Average Compression

| Task | Total Time, wks | N0602 | | | N400 | | | 4457 | | |
|---|---|---|---|---|---|---|---|---|---|---|
| | | Average Compression | | | Average Compression | | | Average Compression | | |
| | | Jet A_4 | Jet A_16 | Jet A_25 | Jet A_4 | Jet A_16 | Jet A_25 | Jet A_4 | Jet A_16 | Jet A_25 |
| Task 2 | 0.0 | 24.1 | 26.1 | 27.7 | 23.9 | 26.1 | 27.3 | 23.3 | 25.2 | 26.3 |
| | 2.0 | 18.5 | 21.1 | 21.8 | 18.6 | 21.0 | 21.7 | 18.5 | 20.8 | 21.2 |
| | 4.0 | 17.1 | 19.7 | 21.1 | 17.4 | 19.6 | 20.8 | 17.5 | 19.9 | 20.6 |
| | 6.0 | 16.3 | 18.5 | 20.4 | 16.4 | 18.7 | 20.1 | 17.1 | 19.1 | 20.2 |
| | 8.0 | 14.9 | 17.8 | 19.5 | 15.4 | 18.0 | 19.5 | 16.1 | 18.7 | 19.4 |
| | 10.0 | 14.1 | 17.3 | 18.8 | 14.6 | 17.5 | 18.7 | 15.7 | 18.1 | 18.9 |
| | 12.0 | 13.5 | 16.6 | 18.4 | 14.2 | 17.0 | 18.3 | 15.2 | 17.7 | 18.3 |
| | 14.0 | 12.6 | 15.7 | 17.6 | 13.6 | 16.4 | 17.6 | 14.5 | 17.0 | 17.7 |
| | 16.0 | 11.9 | 15.1 | 16.8 | 12.8 | 15.5 | 16.8 | 13.9 | 16.3 | 16.9 |
| | 18.0 | 11.4 | 14.5 | 16.2 | 12.3 | 15.0 | 16.4 | 13.6 | 15.8 | 16.4 |
| | 20.0 | 11.2 | 14.1 | 15.8 | 12.2 | 14.6 | 16.0 | 13.4 | 15.5 | 15.9 |
| | 22.0 | 10.4 | 13.3 | 14.9 | 11.4 | 13.8 | 15.3 | 12.8 | 14.9 | 15.1 |
| | 24.0 | 10.3 | 12.7 | 14.4 | 11.2 | 13.4 | 15.0 | 12.4 | 14.4 | 14.6 |
| | 26.0 | 9.7 | 12.2 | 13.6 | 10.8 | 13.2 | 14.4 | 12.0 | 13.8 | 14.1 |
| O-rings removed from the compression fixtures and stored in fuel at room temperature between Tasks 2 and 5 | | | | | | | | | | |
| Task 5 | 28.0 | 12.9 | 15.1 | 16.2 | 13.3 | 16.7 | 18.1 | 13.5 | 16.0 | 17.5 |
| | 30.0 | 10.5 | 12.1 | 12.9 | 11.1 | 13.4 | 14.3 | 12.4 | 14.1 | 15.2 |
| | 32.0 | 10.2 | 11.4 | 12.3 | 10.9 | 12.5 | 13.6 | 11.9 | 13.6 | 14.5 |
| | 34.0 | 10.1 | 10.9 | 11.7 | 10.7 | 12.7 | 12.9 | 12.0 | 13.1 | 13.9 |
| | 36.0 | 9.4 | 10.4 | 11.2 | 10.1 | 12.0 | 12.4 | 11.4 | 12.7 | 13.3 |
| | 38.0 | 9.2 | 9.9 | 10.8 | 9.9 | 11.4 | 11.9 | 11.1 | 12.3 | 12.7 |
| | 40.0 | 9.0 | 9.7 | 10.6 | 9.7 | 11.2 | 11.6 | 10.9 | 12.0 | 12.4 |
| | 42.0 | 9.0 | 9.1 | 10.1 | 9.5 | 10.4 | 11.1 | 10.7 | 11.3 | 12.0 |
| | 44.0 | 8.6 | 9.1 | 9.9 | 9.3 | 10.4 | 10.9 | 10.7 | 11.4 | 11.5 |
| | 46.0 | 8.2 | 8.8 | 9.4 | 9.0 | 10.1 | 10.3 | 10.3 | 11.1 | 11.0 |
| | 48.0 | 8.3 | 8.4 | 9.0 | 9.0 | 9.7 | 9.8 | 10.4 | 10.6 | 10.6 |
| | 50.0 | 8.1 | 8.0 | 8.7 | 8.7 | 9.4 | 9.4 | 9.9 | 10.3 | 10.1 |

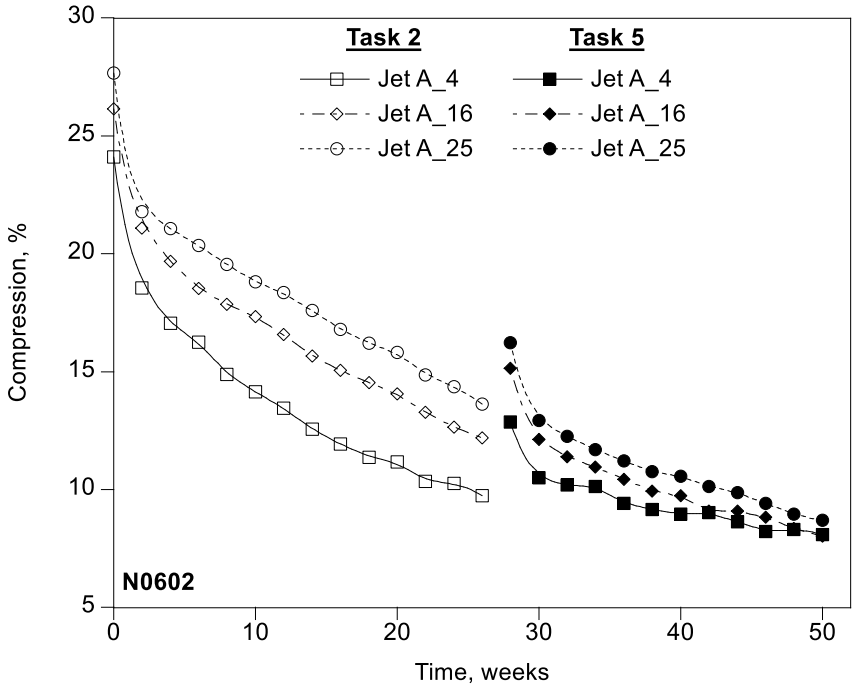


**Figure 32. Compression for the N0602 O-rings as measured during the initial Task 2 and the extended aging in Task 5.**

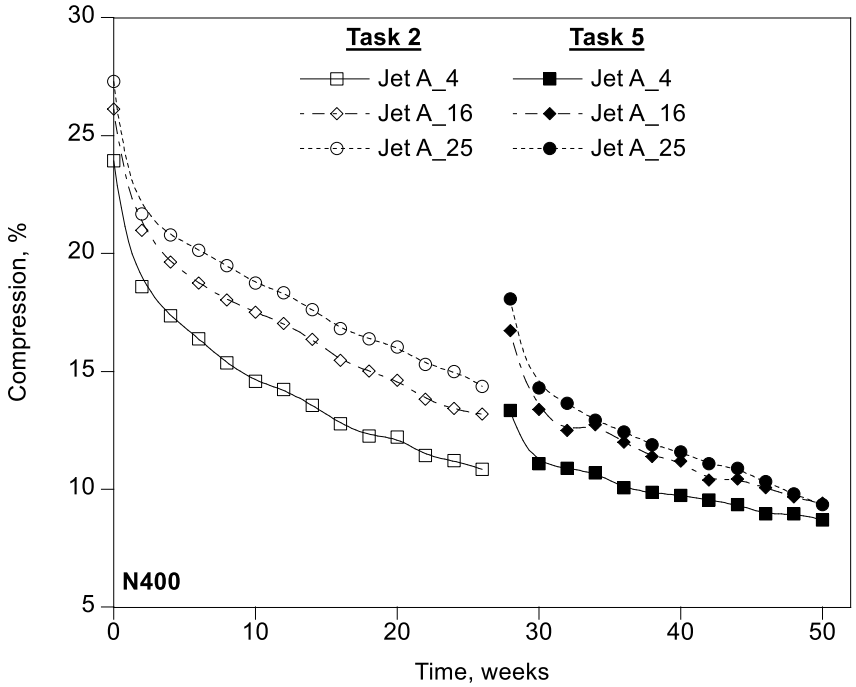


**Figure 33. Compression for the N400 O-rings as measured during the initial Task 2 and the extended aging in Task 5.**

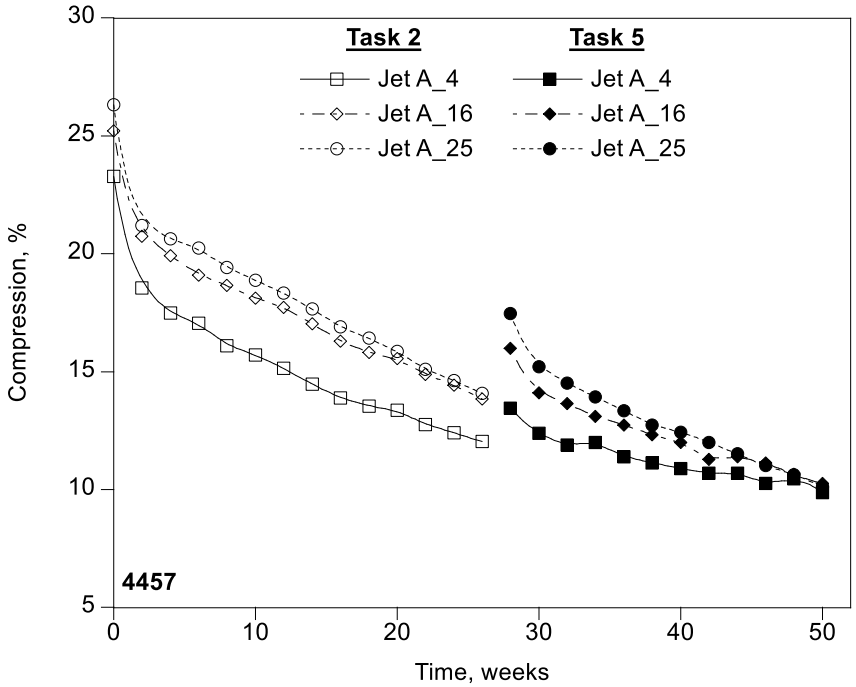


**Figure 34. Compression for the 4457 O-rings as measured during the initial Task 2 and the extended aging in Task 5.**

Prior to leak testing the O-rings were conditioned in the compression fixtures and in their respective conditioning fuels for 1 week at 160˚F starting with 100% SPK. Prior to being installed in the leak test fixture, the test O-rings were installed in an identical fixture and the sealing force was monitored using an Elastocon Compressive Stress Relaxometer to ensure that the O-ring compressive force was at equilibrium prior to the leak test (approximately 30 minutes at room temperature). During the leak test the O-rings were pressurized with the respective conditioning fuels from 5 to 60 psi in 5 psi increments, pausing for 5 minutes at each pressure. (Note that the 60 psi test point was selected based on the reported boost pump pressure from a prior test program with military jet turbine engines.) The sealing pressure was taken as the point where fuel was observed leaking past the seal. The final value given in the tables below were taken as the average of 2 O-rings. This sequence was repeated using 20%, 50%, 80%, and 100% CPK-0 in SPK.

The final test results are summarized in Tables 17, 18, and 19 and Figures 35, 36, and 37 for the O-rings initially aged in Jet A_4, Jet A_16, and Jet A_25, respectively. Note that all of the values given as >60 psi did not leak by the end of the test indicating that the actual sealing pressure was greater than the final pressure of 60 psi. All other values represent the average of 2 O-rings that developed visible leaks during the test and the pressure at which the leaks were observed. Overall, these results show that the O-rings aged in the low aromatic fuel (Jet A_4) performed very well when conditioned in the SPK with 0% CPK-0 with only the N400 giving a sealing pressure of <60 psi and the sealing pressure of these O-rings climbed back above 60 psi when conditioned in the SPK with 20% CPK-0. The O-rings aged in the mid-aromatic fuel (Jet A_16)

showed a modestly degraded performance with the N0602 and N400 O-rings having sealing pressure of <60 psi when conditioned in the neat SPK fuel. These showed improved performance when conditioned in the SPK with 20% CPK-0, and all of the O-rings showed sealing pressures of >60 psi when conditioned in SPK with 50% CPK-0 and higher. The most challenging condition was found for the O-rings that were aged in the high-aromatic fuel (Jet A_25) and then conditioned in the SPK fuel with 0% CPK-0. Under these conditions all of the O-rings showed sealing pressures of <60 psi with the N400 showing the worst overall performance and the N0602 and 4457 showing similar performance. All of the O-rings showed an increase in the sealing pressure as the CPK-0 content of the conditioning fuels increased with the sealing pressure when conditioned in 100% CPK-0 being near, or greater than, 60 psi. These results suggest that aging O-rings in low aromatic fuels does not by itself significantly degrade the performance of a compression seal. However, it is the switch from a modest- to high-aromatic fuel to a low or zero aromatic fuel that degrades the seal performance likely due to the physical change in the dimensions of the O-ring in the direction of compression as a consequence of the fuel switch.

**Table 17 - Measured Sealing Pressure for O-rings Aged in Jet A_4**

| Conditioning Fuel | Sealing Pressure, psi | | |
|---|---|---|---|
| % CPK-0 in SPK | N0602 | N400 | 4457 |
| 0% | >60 | 48 | >60 |
| 20% | >60 | >60 | >60 |
| 50% | >60 | >60 | >60 |
| 80% | >60 | >60 | >60 |
| 100% | >60 | >60 | >60 |

**Table 18 - Measured Sealing Pressure for O-rings Aged in Jet A_16**

| Conditioning Fuel | Sealing Pressure, psi | | |
|---|---|---|---|
| % CPK-0 in SPK | N0602 | N400 | 4457 |
| 0% | 38 | 28 | >60 |
| 20% | 40 | 55 | >60 |
| 50% | >60 | >60 | >60 |
| 80% | >60 | >60 | >60 |
| 100% | >60 | >60 | >60 |

**Table 19 - Measured Sealing Pressure for O-rings Aged in Jet A_25**

| Conditioning Fuel | Sealing Pressure, psi | | |
|---|---|---|---|
| % CPK-0 in SPK | N0602 | N400 | 4457 |
| 0% | 30 | 15 | 45 |
| 20% | 45 | 28 | 45 |
| 50% | 48 | 43 | 50 |
| 80% | 58 | 50 | 48 |
| 100% | >60 | 60 | 58 |

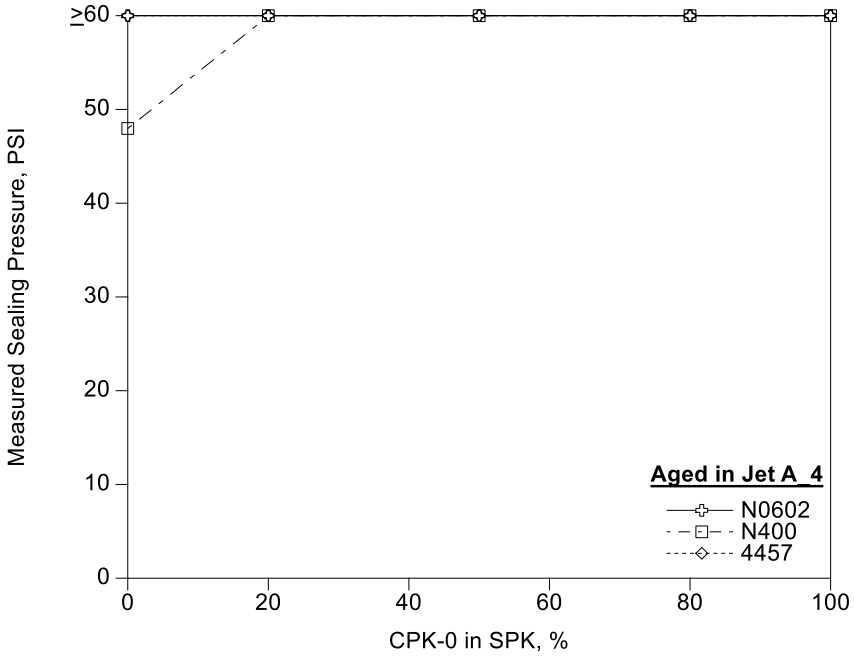


**Figure 35. The measured sealing pressure for O-rings aged in Jet A_4 and then conditioned in blends of CPK-0 in SPK.**

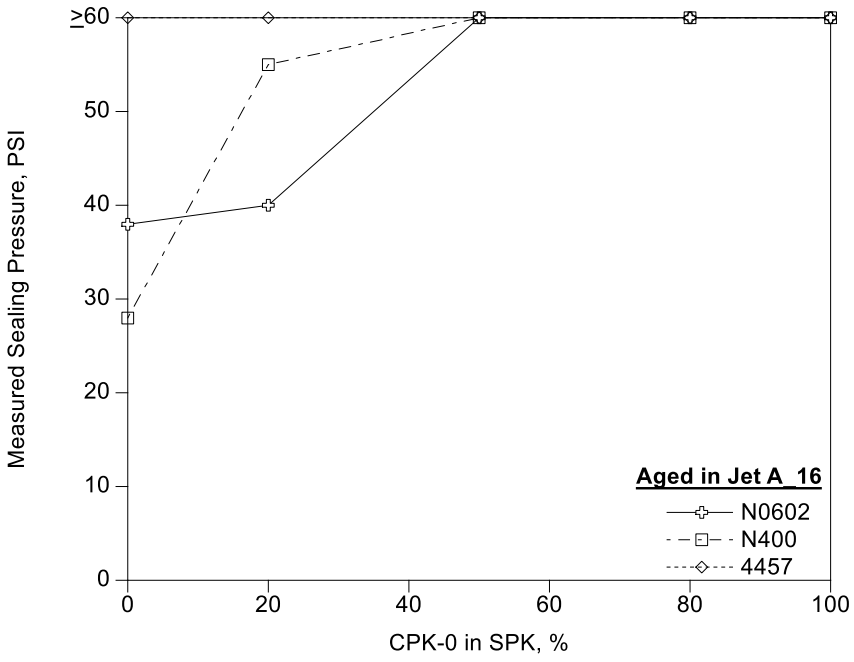


**Figure 36. The measured sealing pressure for O-rings aged in Jet A_16 and then conditioned in blends of CPK-0 in SPK.**

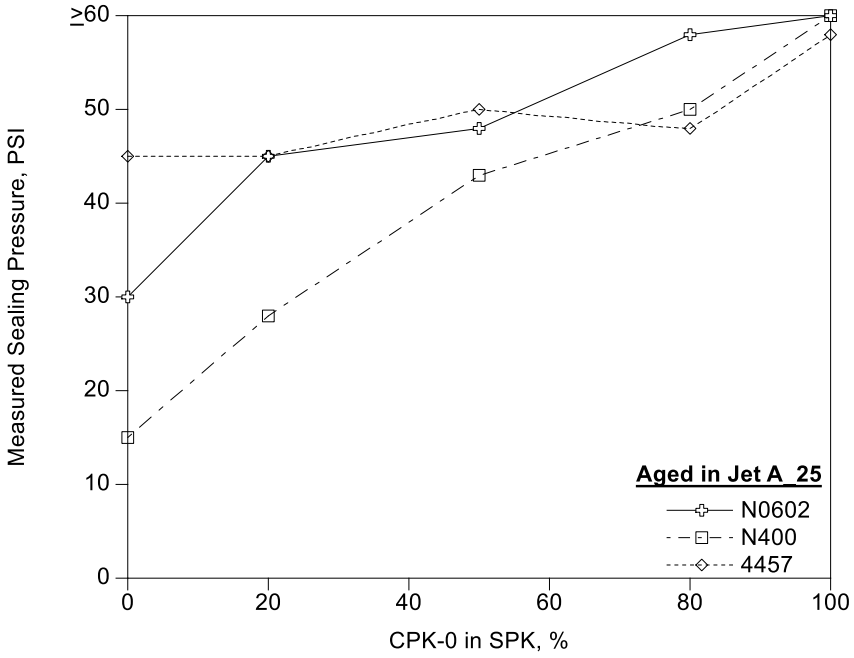


**Figure 37. The measured sealing pressure for O-rings aged in Jet A_25 and then conditioned in blends of CPK-0 in SPK.**

### Task 6 - Compressive Stress Relaxation with Thermal Cycling

In this task the O-ring representing the worst performer from Task 2 (Parker N0602) was mounted in an Elastocon Compressive Stress Relaxometer fitted with a UDRI flow cell at 25% compression and exposed to test fluids for 3000 hours while varying the temperature from +30˚C to -40˚C and back to +30˚C on a 24-hour cycle. This 24-hour "saw tooth" temperature cycle was repeated throughout this test. The compressive stress relaxometer, described below, was fitted with 4 cells and each cell was provided with one of four fuels: Jet A_16 (16.2% aromatics), 100% SPK, 100% CPK, and a blend of SPK with 60% CPK (CPK_60). During this test the compressive stress was continuously monitored and recorded as a function of time and temperature. The data analysis included an examination of the overall compressive stress relaxation and the compressive stress relaxation as a function of time and temperature for each fuel.

In this task the test articles were mounted in an Elastocon Compressive Stress Relaxometer fitted with an O-ring gland as shown in Figures 38 and 39. The fully assembled compressive stress relaxometer is shown in Figure 40. As shown in Figure 38, in a stock compressive stress relaxometer an O-ring is placed between two flat platens and compressed to the level called out for the test (typically 25%). The force required to maintain the compression is measured with a load cell that is incorporated into the thrust rod and the compression frame that forms the relaxometer assembly. In this manner the force required to maintain the compression is measured continuously as a function of time. In its original configuration as shown in Figure 38, the compressive stress relaxometer was designed to monitor the compressive stress relaxation of uniform solid samples such as buttons. While the stock system can be used with O-rings immersed in a test fluid, the flat platens do not restrain the O-ring and the fluid contacting pattern does not match that of a representative service condition. Consequently, the UDRI system was modified

by replacing the bottom platen with a flow cell as shown in Figure 39. This cell holds the O-ring in a gland designed to the nominal specifications for an internally pressurized face seal with 25% compression. The test fluid passes through the inside of the gland providing a wetting pattern comparable to an in-service condition. The flow of fluid through the cell is quite slow (0.5 mL/hr) so that the fuel pressure is negligible as compared to the compressive force and does not interfere with the measurement of the compressive stress relaxation. This trickle flow has been found to be adequate to keep the O-rings wetted during the duration of the test.

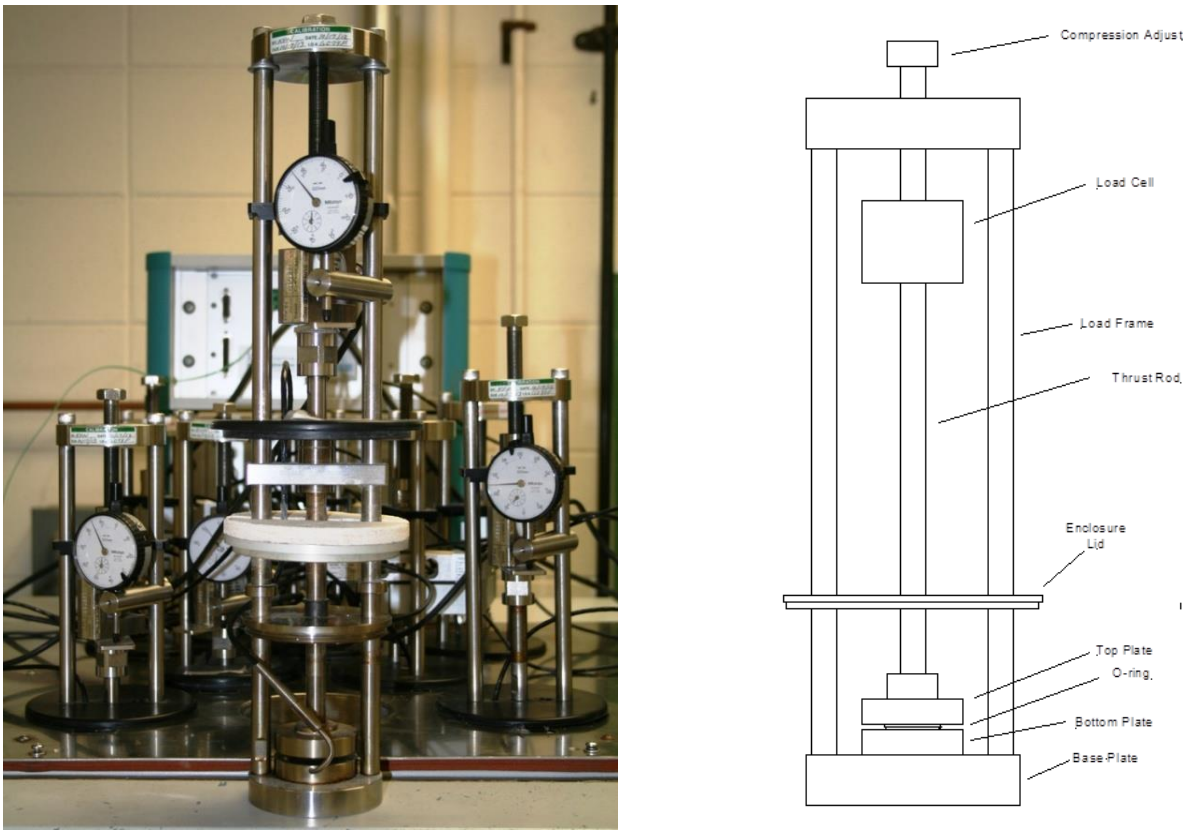


**Figure 38. Photograph (left) and schematic (right) of a stock Elastocon compressive stress relaxometer.**

**Figure 39. Photograph of the modified bottom plate (left) and as installed (right).**


**Figure 40. The assembled compressive stress relaxometer.**

***Test Start and Sample Conditioning***

To start this evaluation the test articles were installed in the relaxometer, the compression frames were lowered into their respective test cells, the fuel lines were installed, and the temperature controller was set to maintain +30˚C. The upper plate was then lowered into contact with each O-ring as indicated by a slight increase in the load being displayed by the data system. The data system was then started, and the compression of each cell was quickly increased to 25% as indicated by the dial gauge incorporated into each cell. The O-rings were allowed to settle in this condition for approximately 21 hours. The flow of fuel was then started for each cell at 20 mL/hour which continued until fuel was observed at the drain from each cell. The flow of fuel continued at this rate until approximately 2 mL of additional fuel had been delivered to each cell, after which the flow of fuel was reduced to 0.5 mL/hour. The O-rings were again allowed to settle under this condition for approximately 21 hours, at which point the temperature cycle was initiated and continued for the next 3,000 hours. During the test the system was closely monitored, and the fuel pumps were refilled on a twice per week schedule.

The relative compressive stress (the force required to maintain a given level of compression normalized by the initial force applied when the O-ring is compressed) during the conditioning period is given in Figure 41. Note that the compressive stress has been normalized by the value at the end of the dry conditioning period, just prior to initiating the flow of fuel to the test cells. This figure shows the typical rapid compressive stress relaxation that occurs with the O-rings are compressed in their respective glands and illustrates how each of the test O-rings relaxed at nearly the same rate. Following a brief transient caused by initiating the fuel flow the O-rings shows varying degrees of response to the fuel and that the magnitude of this response is consistent with the volume swell; SPK < CPK_60 < CPK < Jet A_16. Recall that this behavior is a

response to the simultaneous absorption of fuel by the O-rings, which by itself would cause them to swell and increase the apparent compressive stress, and the extraction of plasticizer, which by itself would cause them to shrink and decrease the apparent compressive stress, the observed behavior being the composite of these two processes. Furthermore, prior work has shown that for O-rings installed in a gland, compressed, and wetted only on their inside radius, this process can be quite slow, taking two weeks or more to reach equilibrium at room temperature.

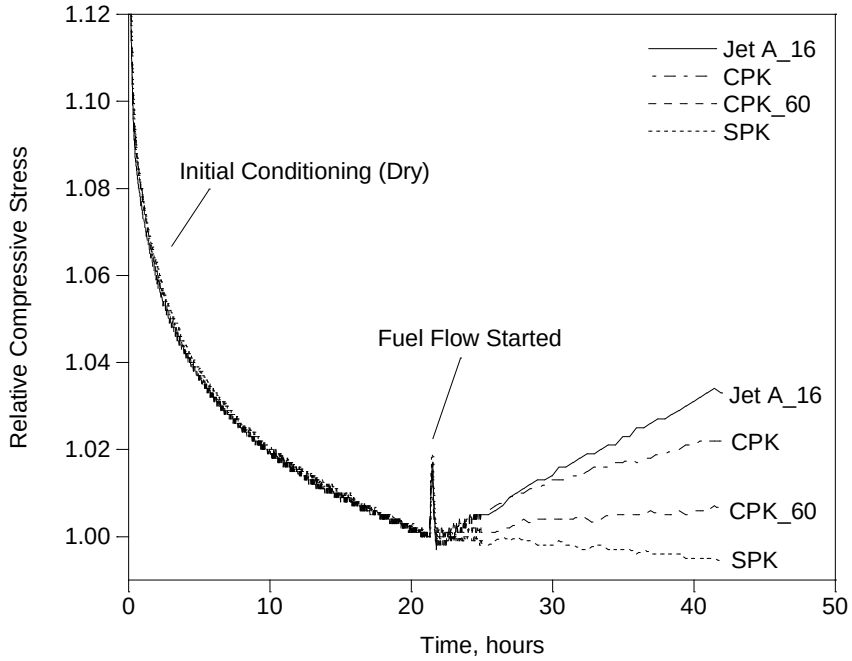


**Figure 41. The relative compressive stress during the initial condition period.**

***Thermal Cycling and Source Data***

A section of the actual temperature measured by thermocouples imbedded in the flow cells is shown in Figure 42. This illustrates the sharp 24-hour cycle that falls just short of the actual target endpoints of +30˚C and -40˚C due to the thermal mass of the test fixtures. The actual average temperature range was +29˚C to -39˚C.

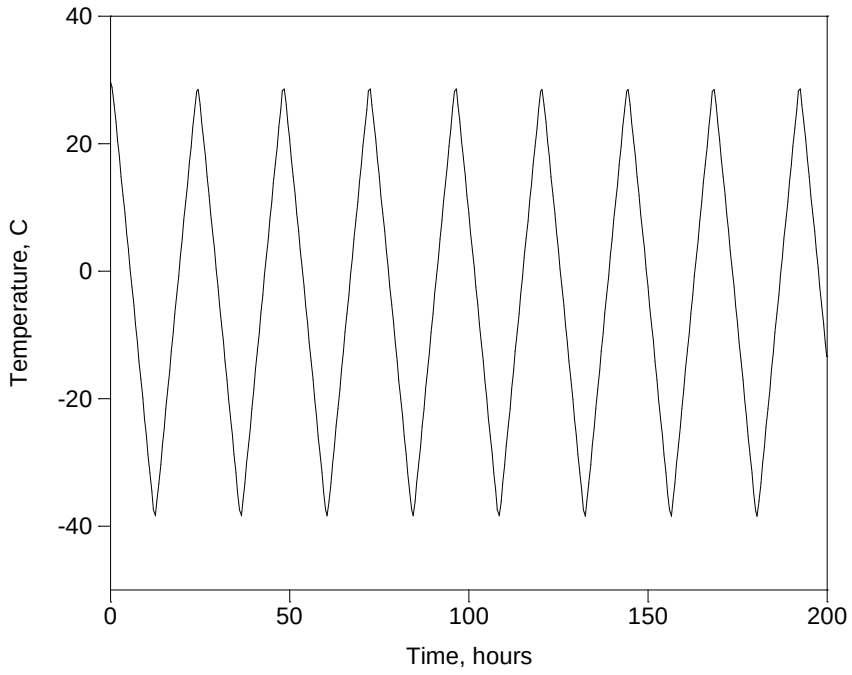


**Figure 42. Example section of the temperature cycle.**

The source data from the compressive stress relaxometer in terms of the relative compressive stress as a function of time is summarized in Figures 43-46 for the O-rings exposed to the Jet A_16, CPK, CPK_60, and SPK, respectively. This order was selected to follow the order of decreasing volume swell as summarized in Table 20. Note that the volume swell of the N0602 O-rings in the CPK_60 and SPK were estimated assuming a linear fit to the volume swell results reported from Task 1. Overall, the behavior of the O-rings in the compressive stress relaxometer track the volume swell results. For example, the relative compressive stress from the O-ring exposed to the Jet A_16 shows an initial period where the compressive stress slowly increases, followed by a prolonged period of gradual decrease. A similar pattern is observed in the CPK_60 and CPK data sets where the initial period of increase fades as the volume swell decreases, and finally the data set with the SPK shows only a gradual loss of compressive stress. In each fluid the rate of compressive stress loss drops to near zero by the end of the testing period, indicating that the rate of relaxation under the test conditions almost ceases. This pattern mimics the volume swell as a function of time as shown in the example for the N0602 from Task 1 given in Figure 47. Briefly, the volume swell for AMS5315 typically shows an initial period of rapid volume swell as the sample quickly absorbs fuel with the concurrent slow extraction of plasticizer followed by a prolonged period of volume loss as the extraction of plasticizer continues. The compressive stress data given in Figures 43-46 show a similar pattern, though the rates are much slower as the O-rings are installed in a gland that is often at low temperature versus fully immersed at room temperature.

**Table 20 – Measured an Estimated Volume Swell**

| Material | Fuel | Swell % v/v | Notes |
|---|---|---|---|
| N0602 | Jet A_16 | 9.8 | From Task 1 |
| | CPK | 4.7 | From Task 1 |
| | CPK_60 | 1.8 | Estimated |
| | SPK | -2.7 | Estimated |

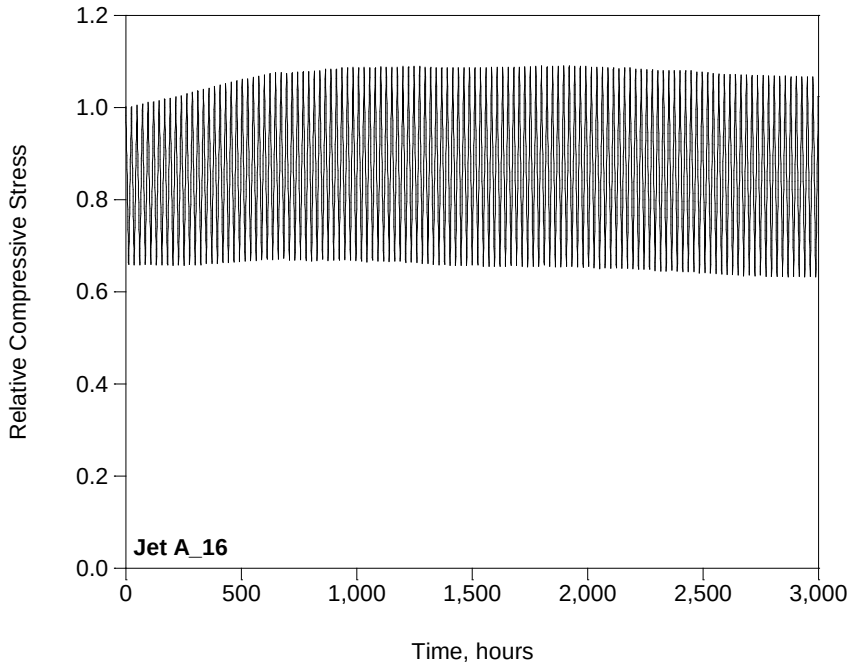


**Figure 43. Summary of the relative compressive stress for the N0602 exposed to the Jet A_16 fuel.**

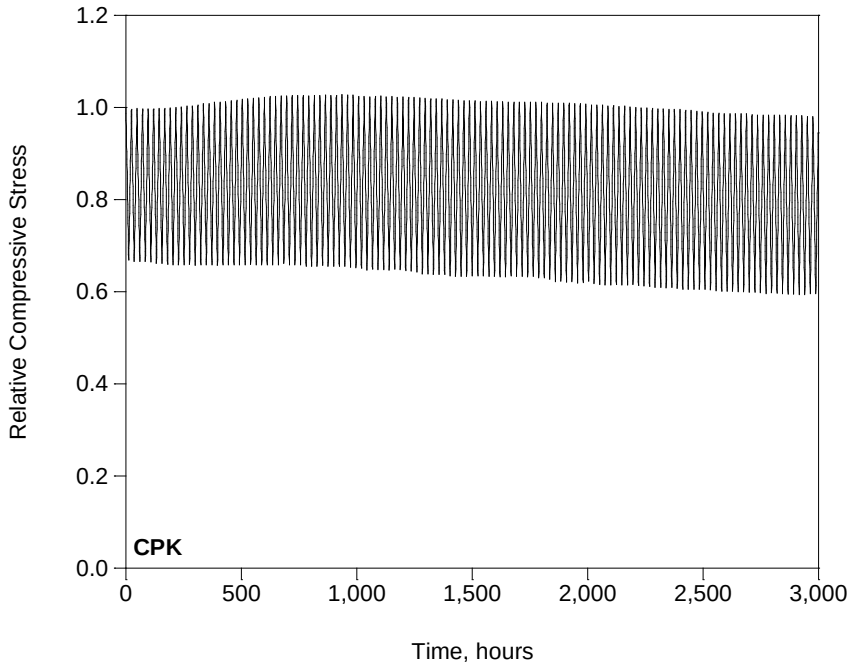


**Figure 44. Summary of the relative compressive stress for the N0602 exposed to the CPK fuel.**

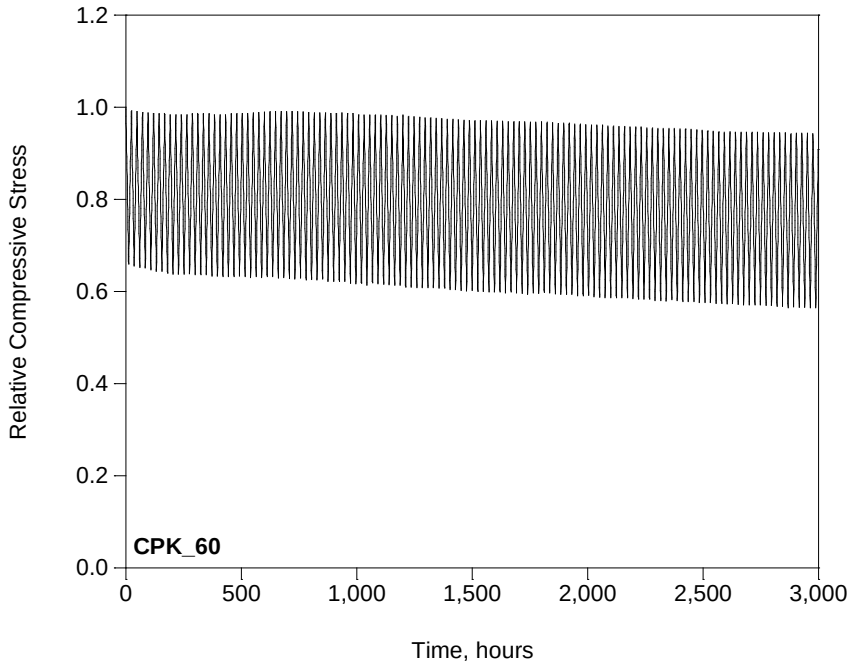


**Figure 45. Summary of the relative compressive stress for the N0602 exposed to the CPK_60 (60% CPK in SPK) fuel.**

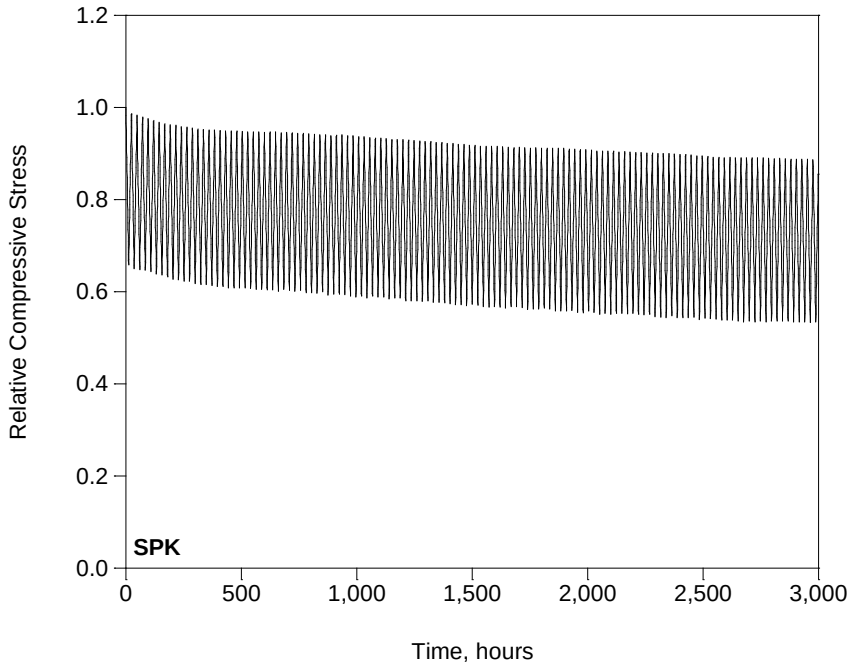


**Figure 46. Summary of the relative compressive stress for the N0602 exposed to the SPK fuel.**

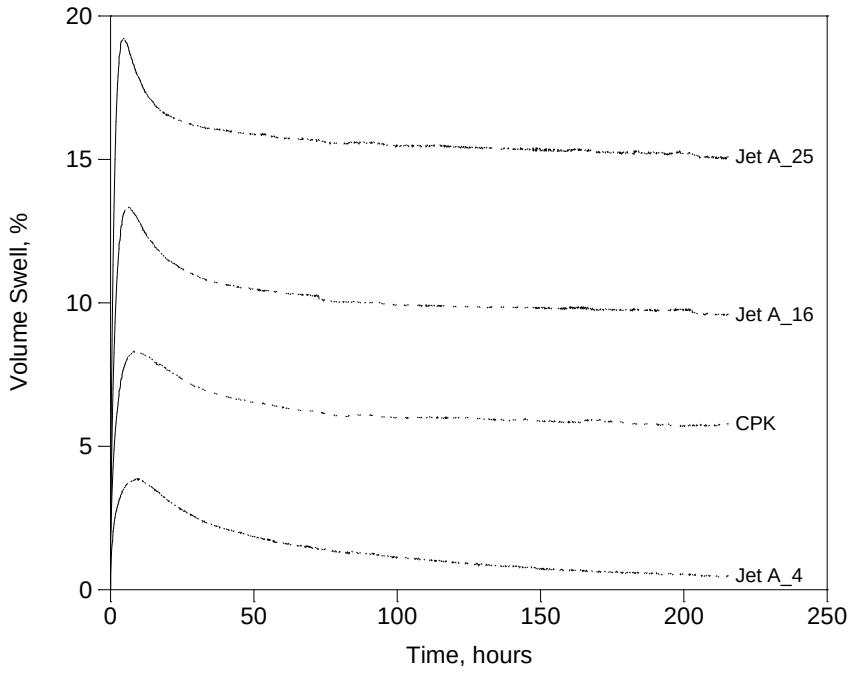


**Figure 47. Example volume swell as a function of time for N0602 from Task 1.**

### *Maximum & Minimum Relative Compressive Stress*

Figure 48 summarizes the source data in terms of the maximum and minimum relative compressive stress measured on each cycle. This makes it easier to compare the results for each of the test fluids. Interestingly, the effect of the fuel is relatively modest as compared to the effect of temperature. For example, the effect of switching between the Jet A_16 and the SPK as shown by the range of maximum (or minimum) values is relatively small compared with the maximum (at +30˚C) and minimum (at -40˚C) values. This suggests that temperature may have a strong influence on seal performance and the potential for transitioning from a sealing condition to a leaking condition.

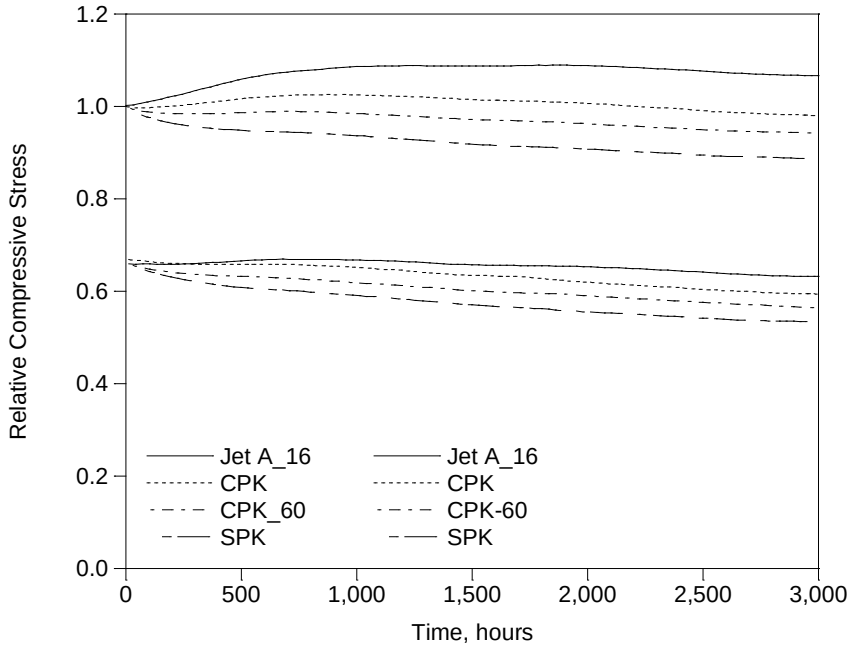


**Figure 48. Summary of the relative compressive stress for the N0602 exposed to the SPK fuel.**

### *Average Compressive Stress Relative to Jet A_16*

Another way to summarize the overall influence of the fuel on the compressive stress is to take the ratio of the measured relative compressive stress (the source data normalized by the initial compressive force) for each of the fuels and normalize it by the relative compressive stress of the O-ring aged with Jet A_16 as shown in Figure 49. The final relative compressive stress values are summarized in Table 21. Figure 50 summarizes these values versus the volume swell values given in Table 20 illustrating a strong correlation between the volume swell (dimensional changes) and the relative compressive stress. This suggests that any changes in the performance of the O-ring seals are likely a consequence of the geometric and physical changes in the O-rings and not irreversible chemical changes in the O-ring material. The slight deviation from linearity in this figure may indicate a change in the volume swell with temperature.

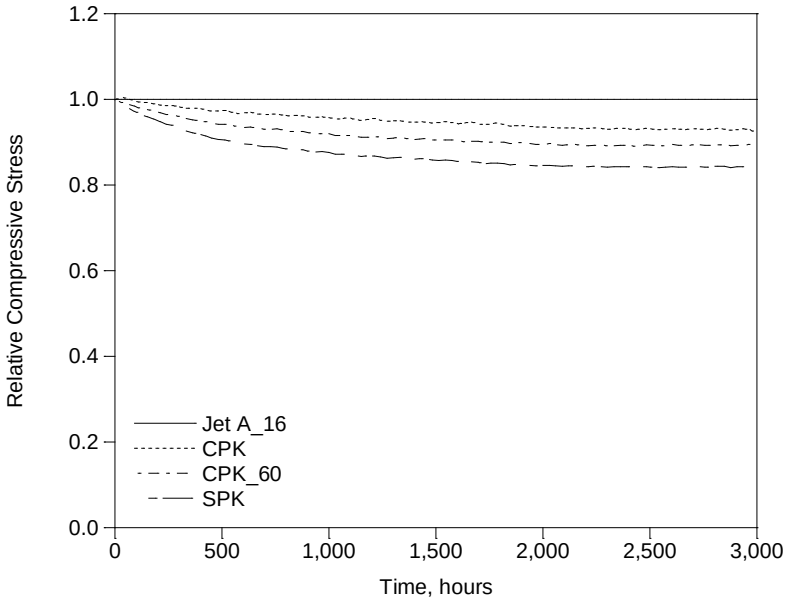


**Figure 49. Summary of the overall compressive.**

**Table 21 – Final Compressive Stress Relative to Jet A_16**

| Fuel | Compressive Stress Relative to Jet A_16 |
|---|---|
| Jet A_16 | 100.0% |
| CPK | 92.9% |
| CPK_60 | 89.3% |
| SPK | 84.2% |

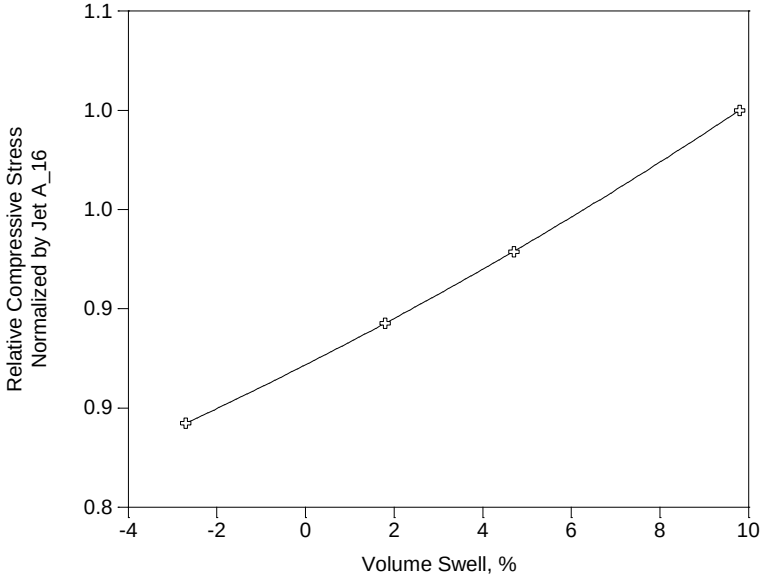


**Figure 50. The final relative compressive stress normalized by the relative compressive stress of Jet A_16 as a function of the volume swell of the test material.**